

Dietary fructose feeds hepatic lipogenesis via microbiota-derived acetate

<https://doi.org/10.1038/s41586-020-2101-7>

Received: 1 February 2019

Accepted: 21 January 2020

Published online: 18 March 2020

 Check for updates

Steven Zhao^{1,2,3,12}, Cholsoon Jang^{4,12}, Joyce Liu^{1,2,5}, Kahealani Uehara^{5,6,7}, Michael Gilbert^{1,2,5}, Luke Izzo^{1,2,3}, Xianfeng Zeng⁴, Sophie Trefely^{1,2,8}, Sully Fernandez^{1,2}, Alessandro Carrer^{1,2,11}, Katelyn D. Miller⁹, Zachary T. Schug⁹, Nathaniel W. Snyder⁸, Terence P. Gade^{1,10}, Paul M. Titchenell^{6,7}, Joshua D. Rabinowitz⁴ & Kathryn E. Wellen^{1,2,7}✉

Consumption of fructose has risen markedly in recent decades owing to the use of sucrose and high-fructose corn syrup in beverages and processed foods¹, and this has contributed to increasing rates of obesity and non-alcoholic fatty liver disease^{2–4}. Fructose intake triggers de novo lipogenesis in the liver^{4–6}, in which carbon precursors of acetyl-CoA are converted into fatty acids. The ATP citrate lyase (ACLY) enzyme cleaves cytosolic citrate to generate acetyl-CoA, and is upregulated after consumption of carbohydrates⁷. Clinical trials are currently pursuing the inhibition of ACLY as a treatment for metabolic diseases⁸. However, the route from dietary fructose to hepatic acetyl-CoA and lipids remains unknown. Here, using in vivo isotope tracing, we show that liver-specific deletion of *Acly* in mice is unable to suppress fructose-induced lipogenesis. Dietary fructose is converted to acetate by the gut microbiota⁹, and this supplies lipogenic acetyl-CoA independently of ACLY¹⁰. Depletion of the microbiota or silencing of hepatic ACS2, which generates acetyl-CoA from acetate, potently suppresses the conversion of bolus fructose into hepatic acetyl-CoA and fatty acids. When fructose is consumed more gradually to facilitate its absorption in the small intestine, both citrate cleavage in hepatocytes and microorganism-derived acetate contribute to lipogenesis. By contrast, the lipogenic transcriptional program is activated in response to fructose in a manner that is independent of acetyl-CoA metabolism. These data reveal a two-pronged mechanism that regulates hepatic lipogenesis, in which fructolysis within hepatocytes provides a signal to promote the expression of lipogenic genes, and the generation of microbial acetate feeds lipogenic pools of acetyl-CoA.

Because ACLY links carbohydrate and lipid metabolism (Extended Data Fig. 1a), we hypothesized that genetic deletion of *Acly* in hepatocytes would protect mice against fructose-induced accumulation of lipids. Although whole-body *Acly* knockout is embryonically lethal¹¹, mice with liver-specific *Acly*-knockout (LAKO) were grossly indistinguishable from wild-type littermate controls, with similar body weights and organ sizes between genotypes on a diet of either standard chow or high fructose (60%) (Extended Data Fig. 1b, c). Fructose consumption triggered mild hepatic accumulation of lipids, without fibrosis or excess accumulation of glycogen, in both wild-type and LAKO mice (Fig. 1a, Extended Data Fig. 1d, e). Metabolomic and lipidomic analyses revealed notable diet-dependent changes and relatively modest genotype-dependent differences (Extended Data Figs. 2a, b, 3a–c, Supplementary Tables 1, 2). Consistent with loss of ACLY activity, the

accumulation of citrate and its downstream metabolite aconitate was observed in livers from LAKO mice (Extended Data Fig. 2c). These data demonstrate that ACLY deficiency, unexpectedly, does not markedly affect global levels of hepatic metabolites or prevent fructose-induced accumulation of triglycerides.

Fructose-driven lipogenesis is ACLY-independent

To further investigate the role of hepatic ACLY in fructose-induced steatosis without altering the overall diet, we fed mice standard chow diets with either normal drinking water or drinking water containing a 1:1 mixture of fructose and glucose (15% each; fructose:glucose) (Extended Data Fig. 4a–c). Similar to mice fed a high-fructose diet, wild-type and LAKO mice drinking fructose:glucose for 4 weeks developed

¹Department of Cancer Biology, University of Pennsylvania Perelman School of Medicine, Philadelphia, PA, USA. ²Abramson Family Cancer Research Institute, University of Pennsylvania Perelman School of Medicine, Philadelphia, PA, USA. ³Cell & Molecular Biology Graduate Group, University of Pennsylvania Perelman School of Medicine, Philadelphia, PA, USA. ⁴Department of Chemistry and Lewis-Sigler Institute for Integrative Genomics, Princeton University, Princeton, NJ, USA. ⁵Biochemistry & Molecular Biophysics Graduate Group, University of Pennsylvania Perelman School of Medicine, Philadelphia, PA, USA. ⁶Department of Physiology, University of Pennsylvania Perelman School of Medicine, Philadelphia, PA, USA. ⁷Institute of Diabetes, Obesity and Metabolism, University of Pennsylvania Perelman School of Medicine, Philadelphia, PA, USA. ⁸Center for Metabolic Disease Research, Department of Microbiology and Immunology, Temple University Lewis Katz School of Medicine, Philadelphia, PA, USA. ⁹Molecular and Cellular Oncogenesis, Wistar Institute, Philadelphia, PA, USA. ¹⁰Department of Radiology, University of Pennsylvania Perelman School of Medicine, Philadelphia, PA, USA. ¹¹Present address: Veneto Institute of Molecular Medicine (VIMM), Padua, Italy. ¹²These authors contributed equally: Steven Zhao, Cholsoon Jang. ✉e-mail: wellenk@upenn.edu

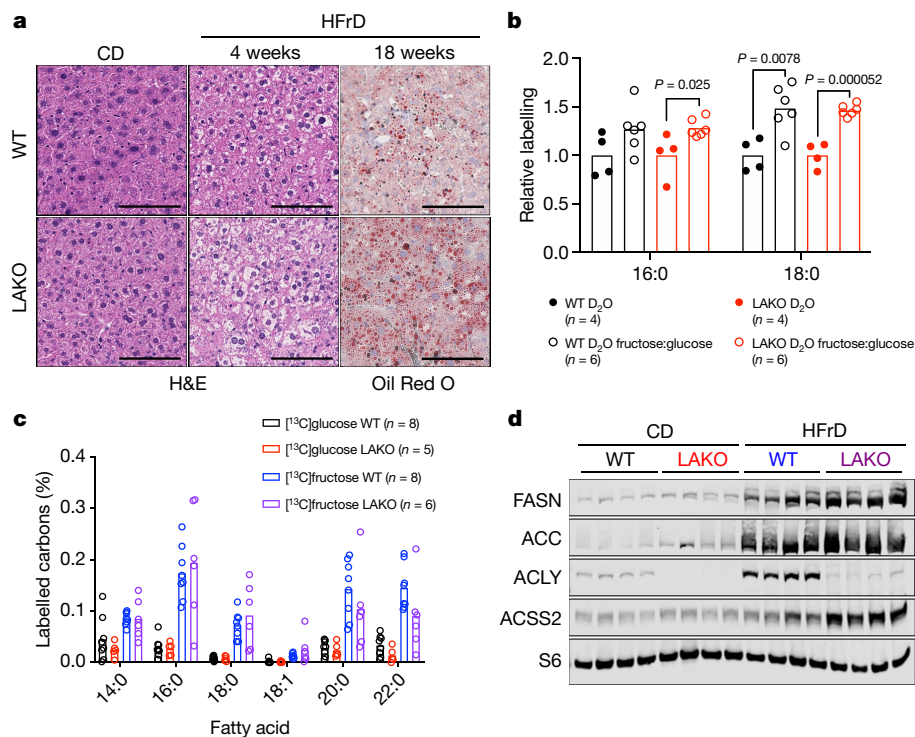


Fig. 1 | Fructose-dependent fatty acid synthesis is ACLY-independent.

a, Representative haematoxylin and eosin (H&E) and Oil Red O histological stains of livers from wild-type (WT) or LAKO mice fed a chow diet (CD) or a high-fructose diet (HFrD) for 4 or 18 weeks. Images are from two independent experiments ($n = 4$ WT and LAKO mice per diet at 4 weeks; and $n = 13$ WT and $n = 6$ LAKO mice per diet at 18 weeks). Scale bars, 100 μm . **b**, Relative deuterium incorporation in saponified palmitic acid (16:0) and stearic acid (18:0) in liver after D_2O labelling of mice for 24 h. The basal level of D_2O labelling is set to

mild hepatic steatosis (Extended Data Fig. 4d). Moreover, deuterated-water (D_2O) tracing revealed that consumption of fructose:glucose increases hepatic de novo lipogenesis (DNL) to a similar extent in wild-type and LAKO mice (Fig. 1b). Thus, the deletion of *Acly* from liver does not prevent DNL in response to fructose consumption.

Given this unexpected result, we directly tested the effect of ACLY deficiency on fructose conversion into nascent fatty acids. Wild-type and LAKO mice were gavaged with 1:1 fructose:glucose, with either glucose or fructose- ^{13}C -labelled (Extended Data Fig. 4e). Notably, fructose carbons were incorporated into fatty acids in LAKO and wild-type mice to a similar extent, whereas glucose carbons were barely used (Fig. 1c, Extended Data Fig. 4f). These data indicate that, in contrast to existing models of fructose metabolism, the use of fructose carbons for hepatic DNL does not require ACLY.

Microbiota-derived acetate feeds lipogenesis

We next investigated the mechanisms of how fructose carbons are used for fatty acid synthesis in an ACLY-independent manner. It has been previously shown that the hepatic DNL program is activated in response to carbohydrate consumption by the ChREBP transcription factor^{12,13}. After chronic high-fructose consumption, the livers of both wild-type and LAKO mice upregulated the highly active ChREBP- β isoform¹⁴, along with lipogenic genes (*Acaca* and *Fasn*) and other ChREBP target genes, aldolase B (*Aldob*), and ketohexokinase (*Khk*)¹⁵ (Extended Data Fig. 5a, b). Wild-type mice on a high-fructose diet also exhibited upregulation of *Acly* (Extended Data Fig. 5a). The induction of the DNL program was also robust at the protein level (Fig. 1d, Extended Data Fig. 5c). The residual ACLY protein in livers from fructose-fed LAKO

1 and compared with D_2O labelling after consumption of fructose:glucose within each genotype. *P* values determined by two-sided *t*-tests. **c**, Percentage of total labelled carbons in saponified fatty acids in serum from mice gavaged with 1:1 fructose:glucose, 1.0 g kg^{-1} of each. ^{13}C -labelled substrates are indicated. Data are mean values. **d**, Western blots of lipogenic enzymes in liver lysates of wild-type or LAKO mice fed a chow or high-fructose diet for 4 weeks. Ribosomal protein S6 was used as a loading control. Data in **c**, **d** are representative of two independent experiments.

mice was detected in cells other than hepatocytes (Extended Data Fig. 5d). Acyl-CoA synthetase short chain family member 2 (ACSS2), which converts acetate into acetyl-CoA, was notably upregulated in fructose-consuming LAKO mice (Fig. 1d, Extended Data Fig. 5b, c). Moreover, the *Acss2* genomic locus showed increased histone H3K27 acetylation after fructose:glucose drinking (Extended Data Fig. 5e). ChREBP binding to the *Acss2* locus was identified in a published chromatin immunoprecipitation with high-throughput sequencing (ChIP-seq) dataset¹⁶ (Extended Data Fig. 5f). *Acss2* is also a target of SREBP transcription factors, which are activated in response to fructose consumption¹⁷⁻¹⁹. These data suggest that ACSS2 is a component of the hepatic response to fructose consumption.

Because the conversion of acetate to acetyl-CoA by ACSS2 can support DNL in the absence of ACLY¹⁰, we proposed that acetate might be an important source of acetyl-CoA for DNL in the context of fructose feeding (Fig. 2a). Acetate can be generated within mammalian cells by several mechanisms²⁰⁻²², prompting us to investigate whether fructose is converted to acetate in a cell-autonomous manner in hepatocytes. Incubation of mouse hepatocytes with 25 mM [^{13}C]fructose labelled fructolytic intermediates (Fig. 2b), but only minimally labelled acetyl-CoA and malonyl-CoA—the core DNL substrates (Fig. 2c). By contrast, 1 mM [^{13}C]acetate was readily used for the synthesis of acetyl-CoA and malonyl-CoA, as well as HMG-CoA—an intermediate in the mevalonate pathway downstream of acetyl-CoA (Fig. 2c). Therefore, even when ACLY is intact, exogenous acetate directly feeds into lipogenic acetyl-CoA pools in hepatocytes.

We thus investigated the possibility that fructose is converted to acetate before reaching the liver to feed hepatic DNL by performing a [^{13}C]fructose isotope-tracing time-course analysis in mice. Oral administration of [^{13}C]fructose labelled both fructose-1-phosphate (F1P) and

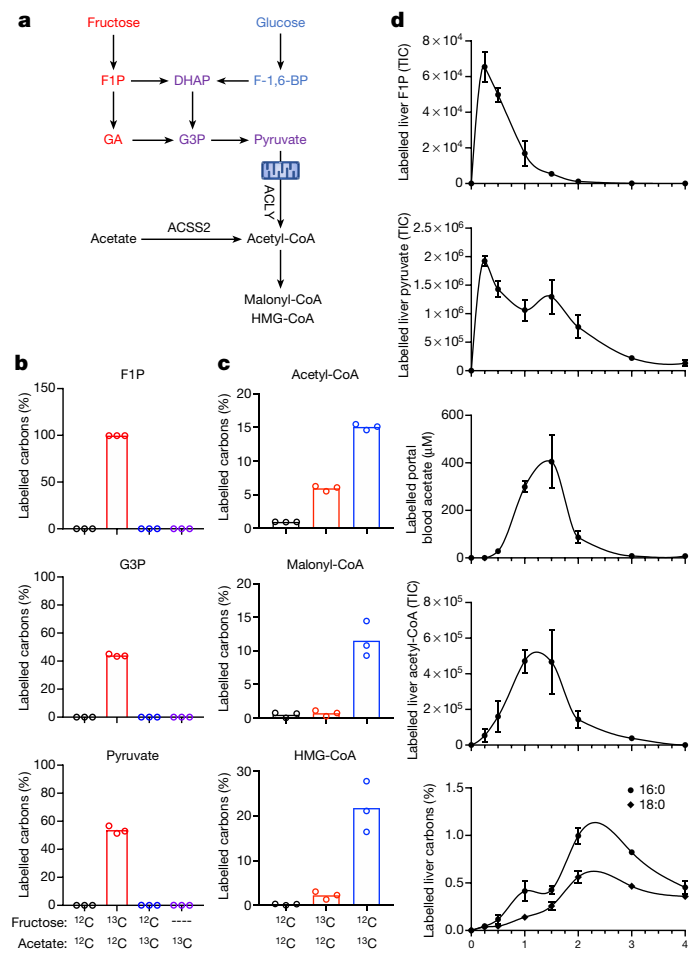


Fig. 2 | Lipogenic acetyl-CoA is preferentially produced from acetate in hepatocytes. **a**, Pathways for lipogenic acetyl-CoA production from fructose, glucose or acetate. F1P, fructose-1-phosphate; DHAP, dihydroxyacetone phosphate; F-1,6-BP, fructose-1,6-bisphosphate; G3P, glyceraldehyde-3-phosphate; GA, glyceraldehyde. **b**, **c**, Percentage of total labelled carbons in fructolytic intermediates (**b**) and acetyl-CoA, malonyl-CoA or HMG-CoA (**c**) in primary hepatocytes incubated for 6 h with 25 mM fructose plus 1 mM acetate. ¹³C-labelled substrates are indicated. Data are mean values. *n* = 3 plates of cells, analysed in parallel. **d**, Total ion counts (TIC) of labelled F1P, pyruvate and acetyl-CoA in liver, concentrations of labelled acetate in the portal blood, and the percentage labelling of saponified palmitic acid (16:0) and stearic acid (18:0) in liver of saline-treated wild-type mice gavaged with 1:1 [¹³C]fructose: unlabelled glucose. Data are mean ± s.e.m. (*n* = 3 mice per time point).

pyruvate in the liver, with peaks between 15 and 30 min after gavage, which indicates rapid absorption of fructose and hepatic fructolysis (Fig. 2d). Hepatic labelling of acetyl-CoA was much slower, peaking at 60–90 min (Fig. 2d). The slower kinetics of acetyl-CoA labelling was closely aligned with the appearance of labelled acetate in the portal circulation (Fig. 2d). Labelling of hepatic fatty acids followed that of acetyl-CoA, peaking at 120–180 min (Fig. 2d), consistent with fructose feeding resulting in the indirect production of hepatic acetyl-CoA and fatty acids via acetate.

We next sought to determine the source of fructose-derived acetate. Although fructose is mainly taken up by the small intestine, unabsorbed fructose reaches the colon where the microbiota converts it into short-chain fatty acids, including acetate⁹. To test whether the microbiota is important for hepatic DNL, we depleted it with an antibiotic cocktail (Extended Data Fig. 6a–d). Antibiotic treatment slightly enhanced the appearance of labelled fructose and fructose-derived glucose in the portal vein after oral administration of [¹³C]fructose

(Extended Data Fig. 6e, f). The induction of hepatic DNL genes after fructose consumption is thought to be dependent on fructolytic and/or glycolytic intermediates^{12,23}. Consistent with the normal passage of fructose from the intestine to the liver, DNL gene expression remained intact after antibiotic treatment (Extended Data Fig. 6g), as did the labelling of F1P, pyruvate and citrate in the liver (Fig. 3a, Extended Data Fig. 7a). By contrast, microbiome depletion markedly reduced the labelling from [¹³C]fructose of hepatic acetyl-CoA and palmitate, as well as fatty acids within circulating lipids (Fig. 3a, b, Extended Data Fig. 7a, b). This reduction was well matched with depleted portal and caecal labelling of acetate and other short-chain fatty acids (Fig. 3a, Extended Data Figs. 7a, 8a, b). Antibiotic treatment also reduced levels of total hepatic triglycerides (Extended Data Fig. 8c), consistent with previous observations^{24,25}. Thus, depletion of microbiota suppresses hepatic DNL from [¹³C]fructose, without impairing fructose metabolism in the small intestine or liver, or the induction of DNL gene expression.

We next investigated whether acetate is a key microbial product supporting DNL. To assess whether fructose intake led to an appreciable increase in concentrations of portal acetate, we measured acetate in portal and systemic serum after gavage. Acetate concentrations in the portal vein increased approximately twofold compared with the baseline (to more than 1 mM) at 60–90 min after fructose gavage (Extended Data Fig. 8d), corresponding to acetate labelling from fructose (Fig. 2d). The rise in portal acetate was absent in antibiotic-treated mice (Extended Data Fig. 8d). Acetate concentrations in the systemic circulation were lower than that in the portal vein and did not markedly fluctuate after fructose consumption, which suggests clearance by the liver (Extended Data Fig. 8d). Next, to assess whether acetate supports DNL downstream of microbial metabolism, mice were gavaged with [¹³C]acetate, along with 1:1 fructose:glucose. DNL from [¹³C]acetate, in contrast to that from [¹³C]fructose, was not affected by antibiotic treatment (Fig. 3c). Finally, to test whether hepatic ACSS2 is required for fructose to feed DNL, ACSS2 in the liver was silenced using an adeno-associated viral (AAV) hairpin targeting *Acss2*²⁶ (Extended Data Fig. 8e–g). Depletion of hepatic ACSS2 strongly suppressed the labelling of fatty acids in circulating lipids from [¹³C]fructose (Fig. 3d). Together, these data point to a two-pronged mechanism of DNL after consumption of a fructose bolus, in which sugar metabolism in hepatocytes triggers the DNL transcriptional program, but microbiome-dependent acetate production serves as the major fructose-derived lipogenic substrate, after conversion to acetyl-CoA by hepatic ACSS2 (Extended Data Fig. 10a).

Distinct lipogenic signal and substrates

Microbiota-dependent acetate production from fructose occurs when the rate of ingestion exceeds the uptake capacity of the small intestine⁹. Thus, if fructose is consumed gradually, its contribution to DNL might occur to a greater extent via ACLY, and to a lesser extent via microbial acetate production. Still, after providing fructose:glucose in the drinking water, DNL was comparably stimulated in the presence or absence of ACLY (Fig. 1b). To explore this further, mice were given ¹³C-labelled fructose or glucose in drinking water for 24 h (Fig. 4a). Fructose-derived carbons provided a substantial contribution to hepatic lipid pools, with greater than 20% of total liver fatty acid carbons being labelled by [¹³C]fructose after 24 h of fructose:glucose drinking, whereas [¹³C]glucose contributed less (Fig. 4b). In this context, ACLY deficiency reduced [¹³C]fructose and [¹³C]glucose labelling of fatty acids (Fig. 4b). Nevertheless, total DNL as measured by D₂O labelling was not different between genotypes (Fig. 4c), indicating sufficient availability of other two-carbon donors. We hypothesized that acetate from other sources (for example, fibre fermentation) might be assimilated. To test this, we supplemented fructose:glucose drinking water with [¹³C]acetate at initial exposure and after 2 weeks on fructose:glucose water (Extended Data Fig. 9a). The labelling of fatty acids from [¹³C]acetate was higher in LAKO mice at baseline (Fig. 4d). After

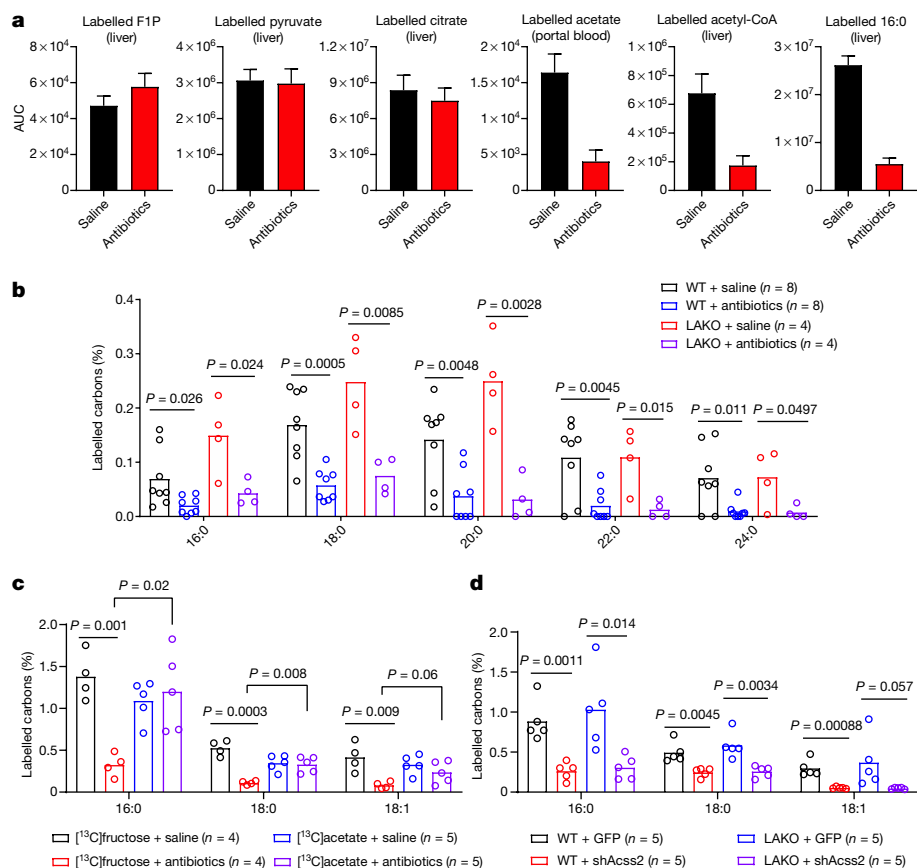


Fig. 3 | Metabolism of bolus fructose by the microbiota feeds hepatic lipogenesis. **a**, Area under curve ($AUC_{0-240 \text{ min}}$) analysis of labelled F1P, pyruvate, citrate, acetyl-CoA and saponified palmitate (16:0) in liver and acetate in portal blood from wild-type mice treated with saline or antibiotics and gavaged with 1:1 [¹³C]fructose:unlabelled glucose. Data are mean \pm s.e.m. See Extended Data Fig. 7a for curves. **b**, Percentage of total labelled carbons in saponified fatty acids in serum from mice treated with saline or antibiotics and gavaged with 1:1 [¹³C]fructose:unlabelled glucose. *P* values determined by two-sided *t*-tests.

c, Percentage of total labelled carbons in saponified fatty acids in serum from LAKO mice treated with saline or antibiotics and gavaged with 1:1 fructose:glucose plus 0.5 g kg⁻¹ acetate. [¹³C]-labelled substrates are indicated. *P* values determined by two-sided *t*-tests. **d**, Percentage of total labelled carbons in saponified fatty acids in serum from 1:1 [¹³C]fructose:unlabelled glucose in wild-type and LAKO mice 1 week after tail vein injection with AAV8-GFP or AAV8-shAcss2. *P* values determined by two-sided *t*-tests. Data in **b-d** denote mean values.

fructose conditioning, the contribution of acetate to DNL increased in wild-type mice, and this was further enhanced in LAKO mice (Fig. 4d), consistent with increased hepatic ACSS2 expression in LAKO mice after fructose feeding, which preceded the onset of steatosis (Extended Data Fig. 9b, c). We next assessed the contribution of microbiome-derived acetate from all dietary sources in the context of gradual fructose consumption. Antibiotic treatment suppressed total hepatic DNL in LAKO mice (Fig. 4e, Extended Data Fig. 9d). ChREBP- β and DNL gene expression were confirmed to be upregulated by fructose:glucose drinking in all groups, indicating that their regulation in response to fructose consumption is independent of acetyl-CoA metabolism (Fig. 4f). Finally, we examined DNL in mice given fructose:glucose after the silencing of hepatic ACSS2, and found that in the context of gradual fructose consumption via drinking water, the loss of both ACLY and ACSS2 is necessary to suppress DNL (Fig. 4g). These data indicate that when fructose is consumed gradually to facilitate its absorption in the small intestine, the rate of DNL is established by signalling mechanisms (that is, sugar-driven activation of ChREBP), and DNL is suppressed only when acetyl-CoA production by both ACLY and ACSS2 is inhibited (Extended Data Fig. 10b).

Discussion

This study demonstrates that bolus fructose consumption triggers hepatic DNL that is independent of liver ACLY but dependent on the

metabolism of fructose by the gut microbiota to acetate, which then reaches the liver via the portal vein. The induction of the DNL transcriptional program in the liver, however, seems to be independent of both ACLY and the microbiome, consistent with evidence that hexose phosphate metabolites are important for ChREBP activation^{19,27}. This may explain why *Khk*-knockout mice are protected from fructose-induced fatty liver^{28,29}. Thus, we propose a revised model of fructose-dependent DNL induction, in which hepatic fructose metabolism provides a signal to promote DNL transcriptionally while microbial fructose metabolism provides acetate to feed DNL (Extended Data Fig. 10a). These dual mechanisms may also explain the higher lipogenic potential of fructose as compared to glucose³⁰, at least in the context of high-dose sugar consumption, in that the small intestine rapidly absorbs even large loads of glucose, whereas fructose reaches the gut microbiota, which generate acetate⁹. When consumed more gradually, fructose can feed DNL in an ACLY-dependent manner. However, acetate from other sources is also readily available to the liver, rendering ACLY dispensable for DNL even when fructose is gradually consumed (Extended Data Fig. 10b). Of note, acetate is probably insufficient to trigger an increase in DNL in the absence of the sugar-derived lipogenic signal. Thus, it will be important to define how fructose interacts with dietary sources of acetate such as ethanol and fermentable fibres.

Understanding the fundamental pathways involved in hepatic DNL is important for the development of therapeutic interventions

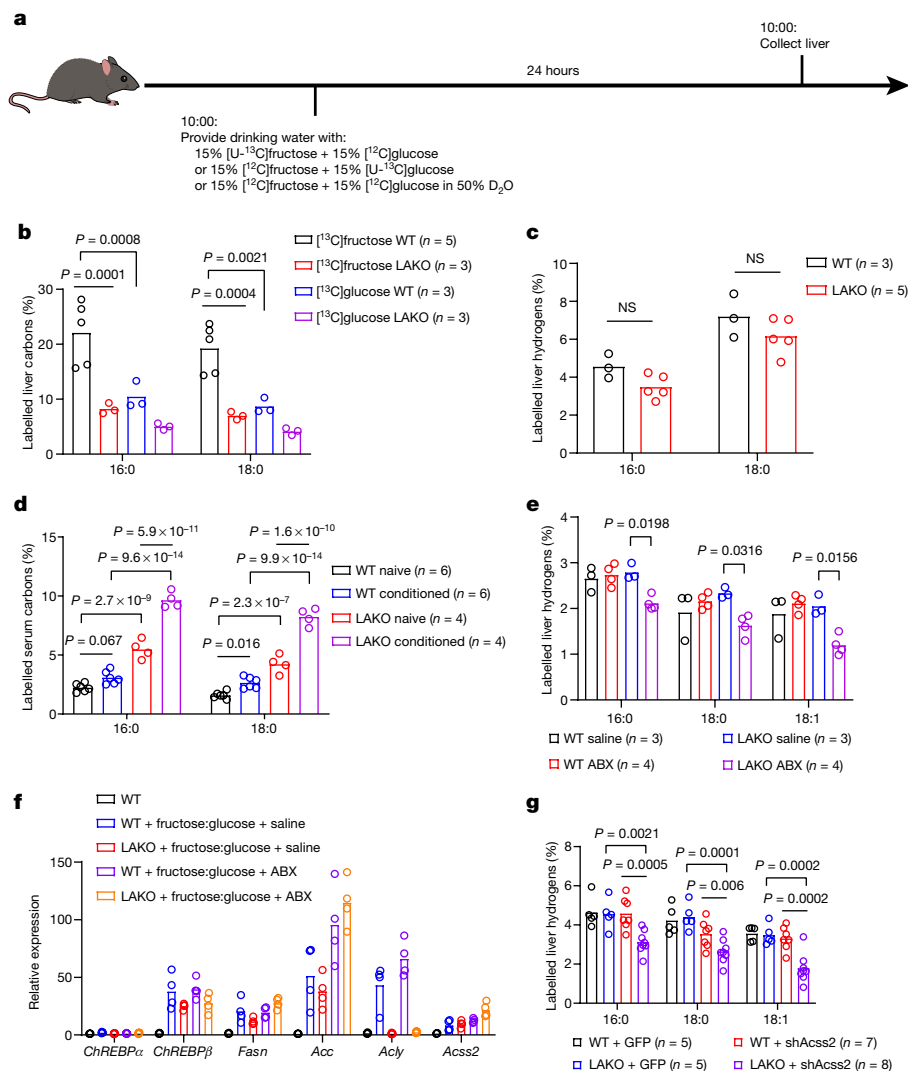


Fig. 4 | Gradual consumption of fructose promotes hepatic lipogenesis from ACLY- and ACSS2-derived acetyl-CoA. **a**, Experimental design for gradual fructose consumption. [¹³C] denotes uniformly labelled ¹³C. **b**, Percentage of total labelled carbons from [¹³C]fructose or [¹³C]glucose in saponified hepatic fatty acids from wild-type or LAKO mice. **c**, Percentage of total labelled hydrogens from D₂O in saponified hepatic fatty acids. **d**, Percentage of total labelled carbons from [¹³C]acetate in saponified fatty acids in serum. See Extended Data Fig. 9a for experimental design. **e**, Percentage of total labelled

hydrogens from D₂O in saponified hepatic fatty acids from wild-type and LAKO mice after treatment with saline or antibiotics (ABX) for 1 week. **f**, mRNA expression of *ChREBP* (also known as *Mlx1pl*) and lipogenic genes in the livers of mice in **e**. **g**, Percentage of total hydrogens labelled in saponified hepatic fatty acids from wild-type and LAKO mice 1 week after injection with AAV8-GFP or AAV8-shAcss2. Data in **b–g** denote mean values. All *P* values determined by two-way analysis of variance (ANOVA) with Tukey's test for multiple comparisons.

for metabolic diseases. In addition to acetate, the microbiome also produces other short-chain fatty acids such as butyrate and propionate. Butyrate has been shown to contribute to hepatic lipogenesis³¹, presumably by first entering the mitochondrial TCA cycle and then feeding extra-mitochondrial pools of acetyl-CoA in an ACLY-dependent manner³². Diet and microbiome could potentially affect the efficacy of ACLY inhibitors, which are currently in clinical trials for hypercholesterolaemia³³. Previous studies of RNA-interference-mediated ACLY deficiency report decreased hepatic lipids in *db/db* mice and mice fed a high-fat, high-sucrose diet, but increased hepatic lipids in mice fed a high-fat diet only^{34–36}. In our own data, principal component analysis of hepatic triglycerides separated LAKO mice from wild-type mice on a high-fructose but not a chow diet (Extended Data Fig. 3c), supporting the notion that ACLY may have distinct roles depending on diet. The current data determine a previously unappreciated interaction between diet, the gut microbiome, and host organ metabolism that contributes to fructose-induced non-alcoholic fatty liver disease.

Online content

Any methods, additional references, Nature Research reporting summaries, source data, extended data, supplementary information, acknowledgements, peer review information; details of author contributions and competing interests; and statements of data and code availability are available at <https://doi.org/10.1038/s41586-020-2101-7>.

- Bray, G. A., Nielsen, S. J. & Popkin, B. M. Consumption of high-fructose corn syrup in beverages may play a role in the epidemic of obesity. *Am. J. Clin. Nutr.* **79**, 537–543 (2004).
- Jensen, T. et al. Fructose and sugar: A major mediator of non-alcoholic fatty liver disease. *J. Hepatol.* **68**, 1063–1075 (2018).
- Hannou, S. A., Haslam, D. E., McKeown, N. M. & Herman, M. A. Fructose metabolism and metabolic disease. *J. Clin. Invest.* **128**, 545–555 (2018).
- Softic, S., Cohen, D. E. & Kahn, C. R. Role of dietary fructose and hepatic de novo lipogenesis in fatty liver disease. *Dig. Dis. Sci.* **61**, 1282–1293 (2016).
- Lambert, J. E., Ramos-Roman, M. A., Browning, J. D. & Parks, E. J. Increased de novo lipogenesis is a distinct characteristic of individuals with nonalcoholic fatty liver disease. *Gastroenterology* **146**, 726–735 (2014).
- Donnelly, K. L. et al. Sources of fatty acids stored in liver and secreted via lipoproteins in patients with nonalcoholic fatty liver disease. *J. Clin. Invest.* **115**, 1343–1351 (2005).

7. Fukuda, H., Katsurada, A. & Iritani, N. Effects of nutrients and hormones on gene expression of ATP citrate-lyase in rat liver. *Eur. J. Biochem.* **209**, 217–222 (1992).
8. Pinkosky, S. L., Groot, P. H. E., Lalwani, N. D. & Steinberg, G. R. Targeting ATP-Citrate Lyase in Hyperlipidemia and Metabolic Disorders. *Trends Mol. Med.* **23**, 1047–1063 (2017).
9. Jang, C. et al. The small intestine converts dietary fructose into glucose and organic acids. *Cell Metab.* **27**, 351–361.e3 (2018).
10. Zhao, S. et al. ATP-citrate lyase controls a glucose-to-acetate metabolic switch. *Cell Rep.* **17**, 1037–1052 (2016).
11. Beigneux, A. P. et al. ATP-citrate lyase deficiency in the mouse. *J. Biol. Chem.* **279**, 9557–9564 (2004).
12. Herman, M. A. & Samuel, V. T. The sweet path to metabolic demise: fructose and lipid synthesis. *Trends Endocrinol. Metab.* **27**, 719–730 (2016).
13. Uyeda, K. & Repa, J. J. Carbohydrate response element binding protein, ChREBP, a transcription factor coupling hepatic glucose utilization and lipid synthesis. *Cell Metab.* **4**, 107–110 (2006).
14. Herman, M. A. et al. A novel ChREBP isoform in adipose tissue regulates systemic glucose metabolism. *Nature* **484**, 333–338 (2012).
15. Iizuka, K. The role of carbohydrate response element binding protein in intestinal and hepatic fructose metabolism. *Nutrients* **9**, 181 (2017).
16. Pongvarin, N. et al. Genome-wide analysis of ChREBP binding sites on male mouse liver and white adipose chromatin. *Endocrinology* **156**, 1982–1994 (2015).
17. Luong, A., Hannah, V. C., Brown, M. S. & Goldstein, J. L. Molecular characterization of human acetyl-CoA synthetase, an enzyme regulated by sterol regulatory element-binding proteins. *J. Biol. Chem.* **275**, 26458–26466 (2000).
18. Ikeda, Y. et al. Transcriptional regulation of the murine acetyl-CoA synthetase 1 gene through multiple clustered binding sites for sterol regulatory element-binding proteins and a single neighboring site for Sp1. *J. Biol. Chem.* **276**, 34259–34269 (2001).
19. Softic, S. et al. Divergent effects of glucose and fructose on hepatic lipogenesis and insulin signaling. *J. Clin. Invest.* **127**, 4059–4074 (2017).
20. Liu, X. et al. Acetate production from glucose and coupling to mitochondrial metabolism in mammals. *Cell* **175**, 502–513.e13 (2018).
21. Bulusu, V. et al. Acetate recapturing by nuclear acetyl-coa synthetase 2 prevents loss of histone acetylation during oxygen and serum limitation. *Cell Rep.* **18**, 647–658 (2017).
22. Lu, M. et al. ACO12-dependent alteration of acetyl-coa drives hepatocellular carcinoma metastasis by epigenetic induction of epithelial-mesenchymal transition. *Cell Metab.* **29**, 886–900.e5 (2019).
23. Ter Horst, K. W. & Serlie, M. J. Fructose consumption, lipogenesis, and non-alcoholic fatty liver disease. *Nutrients* **9**, 981 (2017).
24. Bergheim, I. et al. Antibiotics protect against fructose-induced hepatic lipid accumulation in mice: role of endotoxin. *J. Hepatol.* **48**, 983–992 (2008).
25. Kaden-Volynets, V. et al. Lack of liver steatosis in germ-free mice following hypercaloric diets. *Eur. J. Nutr.* **58**, 1933–1945 (2019).
26. Mews, P. et al. Acetyl-CoA synthetase regulates histone acetylation and hippocampal memory. *Nature* **546**, 381–386 (2017).
27. Li, M. V. et al. Glucose-6-phosphate mediates activation of the carbohydrate responsive binding protein (ChREBP). *Biochem. Biophys. Res. Commun.* **395**, 395–400 (2010).
28. Lanaspá, M. A. et al. Ketohehexokinase C blockade ameliorates fructose-induced metabolic dysfunction in fructose-sensitive mice. *J. Clin. Invest.* **128**, 2226–2238 (2018).
29. Ishimoto, T. et al. Opposing effects of fructokinase C and A isoforms on fructose-induced metabolic syndrome in mice. *Proc. Natl Acad. Sci. USA* **109**, 4320–4325 (2012).
30. Parks, E. J., Skokan, L. E., Timlin, M. T. & Dingfelder, C. S. Dietary sugars stimulate fatty acid synthesis in adults. *J. Nutr.* **138**, 1039–1046 (2008).
31. den Besten, G. et al. Gut-derived short-chain fatty acids are vividly assimilated into host carbohydrates and lipids. *Am. J. Physiol. Gastrointest. Liver Physiol.* **305**, G900–G910 (2013).
32. Donohoe, D. R. et al. The Warburg effect dictates the mechanism of butyrate-mediated histone acetylation and cell proliferation. *Mol. Cell* **48**, 612–626 (2012).
33. Ziegelbaum, N. K., Yandrapalli, S., Nabors, C. & Frishman, W. H. Bempedoic acid (ETC-1002): ATP citrate lyase inhibitor: review of a first-in-class medication with potential benefit in statin-refractory cases. *Cardiol. Rev.* **27**, 49–56 (2019).
34. Guo, L. et al. Enhanced acetylation of ATP-citrate lyase promotes the progression of nonalcoholic fatty liver disease. *J. Biol. Chem.* **294**, 11805–11816 (2019).
35. Wang, Q. et al. Abrogation of hepatic ATP-citrate lyase protects against fatty liver and ameliorates hyperglycemia in leptin receptor-deficient mice. *Hepatology* **49**, 1166–1175 (2009).
36. Wang, Q. et al. Deficiency in hepatic ATP-citrate lyase affects VLDL-triglyceride mobilization and liver fatty acid composition in mice. *J. Lipid Res.* **51**, 2516–2526 (2010).

Publisher's note Springer Nature remains neutral with regard to jurisdictional claims in published maps and institutional affiliations.

© The Author(s), under exclusive licence to Springer Nature Limited 2020

Article

Methods

Data reporting

No statistical methods were used to predetermine sample size. The experiments were not randomized and investigators were not blinded to allocation during experiments and outcome assessment.

Generation of LAKO mice

Generation of *Acly*^{fl/fl} mice on a C57Bl6/J background was previously described¹⁰. To generate hepatocyte-specific *Acly* knockouts, *Acly*^{fl/fl} mice were crossed to albumin-Cre transgenic mice (B6.Cg^{Tg(Alb-cre)21Mgn/J}, Jackson Laboratory)³⁷.

Genotyping

Genotyping of the recombined *Acly* allele was confirmed as previously described¹⁰. Genotyping of the *Alb-cre* allele was confirmed with the following primer sequences: *Alb-cre-5'F* (CCTGCCAGCATGGATATAA), *Alb-cre-3'R* (GTTGTCTTTGTGCTGCTGA), *Alb-TSP3* (GAAGCAGAAGCT-TAGGAAGATGG), and the following cycling conditions: 1 cycle at 94 °C for 5 min; 35 cycles at 94 °C for 45 s, 58 °C for 45 s, 72 °C for 1 min; and 1 cycle at 72 °C for 10 min; hold at 4 °C.

Mouse studies

All animal protocols in this study were approved by the University of Pennsylvania's Institutional Animal Care and Use Committee (IACUC) and Princeton University's IACUC. For diet studies, 4-week-old male mice were placed on either a regular chow diet (Lab Diet 5010) or a high-fructose chow diet (Teklad TD.89247) for indicated lengths of time. Weights of mice kept on each diet were taken weekly. For drinking-water studies, mice were provided with regular tap water (filtered through a 0.22- μ m filter) or 15% (w/v) fructose:15% (w/v) glucose (Sigma F3510, G8270) in tap water (filtered through a 0.22- μ m filter). Daily water consumption was determined by measuring the total consumption in a cage, divided by the number of mice in the cage. To deplete the gut microbiome, mice were given a daily 10 μ l g⁻¹ body weight oral gavage consisting of 1 mg ml⁻¹ ampicillin, 1 mg ml⁻¹ gentamicin, 0.5 mg ml⁻¹ vancomycin, 1 mg ml⁻¹ neomycin, 1 mg ml⁻¹ metronidazole in a 0.9% NaCl solution for 7–10 days. Studies were controlled to mice given the same 0.9% NaCl solution without antibiotics. To knockdown *Acss2*, 6–8-week-old male mice were injected via tail-vein with 2.0×10^{11} genome copies per mouse of AAV8.U6.shAcss2.CMV.eGFP.SV40 (University of Pennsylvania Vector Core) or AAV8.CMV.PI.eGFP.WPRE.bGH (Addgene) as a control; experiments were performed 1 week after injection.

Histology

For H&E, Periodic Acid Schiff and trichrome staining: tissues were fixed in formalin overnight, dehydrated by titrating in ethanol (50%, 75% and 95%), and submitted to the Molecular Pathology and Imaging Core at the University of Pennsylvania for paraffin embedding, sectioning and staining. For Oil Red O staining: tissues were fixed in formalin overnight, dehydrated by titrating in sucrose (10%, 20% and 30%), and embedded in Richard-Allan Scientific NEG-50 frozen section medium (ThermoFisher Scientific, 6502) by freezing in 2-methylbutane that was cooled using dry ice. Tissues frozen in NEG-50 were submitted to the Molecular Pathology and Imaging Core at the University of Pennsylvania for cryosectioning and staining. Images were acquired on a Keyence BZ-X710 microscope.

Bacterial quantification

Caecal contents were collected, snap-frozen and weighed before storage at -80 °C until use. DNA was extracted from caecal contents using a Fecal DNA extraction kit (IBI Scientific, IB47821) according to manufacturer's instructions. Samples were diluted 1:1,000 before use for reverse transcription PCR (RT-PCR). To establish a bacterial DNA standard, genomic DNA was extracted from Stb13 *E. coli* cells. A

standard curve was generated using a 1:4 serial dilution starting with 10 ng of *E. coli* DNA. RT-PCR was performed as described, using previously published universal *I6S* primers (forward: 5'-TCCTACGGGAGGC AGCAGT-3', reverse: 5'-GGACTACCAGGTATCTAATCTGTT-3')³⁸. Relative bacterial load was calculated by normalizing DNA content to initial caecal content weight.

Western blotting

Protein extraction from tissue was performed by re-suspending frozen tissue in 0.5 ml of RIPA buffer (1% NP-40, 0.5% deoxycholate, 0.1% SDS, 150 mM NaCl, 50 mM Tris plus protease and phosphatase inhibitors), and lysed using a tissue lyser (Qiagen) twice for 30 s at 20 Hz. After lysis, samples were incubated on ice for 10 min, then spun down at 15,000g for 5 min at 4 °C. Supernatant was collected and stored in -80 °C until immunoblotting. Antibodies used in this study were: ACY1 (Proteintech, 15421-1-AP), ACS2 (Cell Signaling Technology, 3658S), acetyl-CoA carboxylase (Cell Signaling Technology, 3676S), fatty acid synthase (Cell Signaling Technology 3189S), catalase (Cell Signaling Technology, 14097S), ribosomal protein S6 (Cell Signaling Technology 2217S), and IRDye800CW goat anti-rabbit (LI-COR 926-32211). Immunoblots were developed using a LI-COR Odyssey Clx.

RT-qPCR

RNA extraction from tissue was performed by re-suspending frozen tissue in 1 ml Trizol (Life Technologies), and lysed using a tissue lyser (Qiagen) for 60 s at 30 Hz, followed by manufacturer protocol for Trizol RNA extraction. cDNA was synthesized using high-capacity RNA-to-cDNA master mix (Applied Biosystems, 4368814), as per the kit instructions. cDNA was diluted 1:20 and amplified using PowerUp SYBR Green Master Mix (Applied Biosystems, A25778) on the ViiA-7 Real-Time PCR system. Fold change in expression was calculated using ΔC_t , with the *18S* reference gene as an endogenous control. Primer sequences for RT-qPCR are: *Aldob* (forward: GAAACCGCTGCAAAGGATAA, reverse: GAGGCTCTCGTGGAAAAGGAT), *Khk* (forward: ATGTGGTGGCAAATACCCAGA, reverse: CAAGCAAGGAAAGGACAGTGC), *Acly* (forward: TTCGTCAAACAGCACTTCC, reverse: ATTTGGCTTCTTGGAGGTG), *Acss2* (forward: GCTTCTTTCCATTCTTCGGT, reverse: CCCGGA CTCATTACAGGATTG), *ChREBPa* (forward: CGACACTCACCCACCTCTTC, reverse: TTGTTCAGCCGATCTTGTG), *ChREBPb* (forward: TCTGCAGATCGCGTGGAG, reverse: CTTGTCCCGGCATAGCAAC), *Fasn* (forward: ATGGTGGTGTGGACATGGTC, reverse: CCCAGCCTTCCATCTCCTG), *Acc1* (forward: ACAGTGGAGCTAGAATTGGAC, reverse: ACTTCCCGACCA AGGACTTTG).

Measurement of DNL using isotope tracers

To assess total lipogenesis, mice were provided with 50% (v/v) deuterated water (Sigma 151882) mixed into 15% fructose:15% glucose (w/v) drinking water for 24 h. Systemic blood was collected by cardiac puncture, allowed to coagulate on ice for 15 min, and spun down at 15,000g for 10 min at 4 °C to collect serum. To account for differences in drinking water consumption, calculated deuterium enrichment labelling in serum water was used to normalize labelling into fatty acids. To assess lipogenesis from dietary carbohydrates, on the day of experiment, mice were weighed and fasted from 10:00 until 15:00, when they were given an oral gavage consisting of a 1:1 mixture of glucose and fructose in 0.9% NaCl saline. Doses used in this study ranged from 1.0 g kg⁻¹ or 2.0 g kg⁻¹ of each hexose. [¹³C]glucose (Cambridge Isotope Laboratories, CLM-1396-1) or [¹³C]fructose (Cambridge Isotope Laboratories, CLM-1553-1) were provided with the corresponding unlabelled hexose. Six hours after gavage, systemic blood was collected by tail bleeding the mice and incubating the blood on ice for 15 min before spinning down at 15,000g for 10 min at 4 °C to collect serum. To assess lipogenesis from dietary acetate, this procedure was repeated, but with an oral gavage containing 2.0 g kg⁻¹ of unlabelled glucose and fructose with 0.5 g kg⁻¹ [1,2-¹³C]acetate

(Cambridge Isotope Laboratories, CLM-440-1). To assess lipogenesis from dietary carbohydrates in drinking water, [U - ^{13}C]glucose or [U - ^{13}C]fructose were provided with the corresponding unlabeled hexose at 15% (w/v) in drinking water for 24 h. To assess lipogenesis from dietary acetate in drinking water, 150 mM [$1,2$ - ^{13}C]acetate was added to 15% fructose:15% glucose (w/v) for 24 h. Tissues were collected using a clamp pre-cooled with liquid nitrogen. The frozen liver samples were ground at liquid nitrogen temperature with a Cryomill (Retsch). Saponification of lipids and liquid chromatography–mass spectrometry (LC–MS) analysis were performed as previously described³⁹. In brief, serum (5 μ l) or liver powder (10 mg) was incubated with 1 ml of 0.3 M KOH in 90% methanol at 80 °C for 1 h in a 2 ml glass vial. Formic acid (0.1 ml) was then added for neutralization. The saponified fatty acids were extracted by adding 0.5 ml of hexane, vortexing, and transferring the top hexane layer to a new glass vial. Samples were then dried under a stream of nitrogen gas and dissolved in 100 μ l (for serum) or 1 ml (for liver) of isopropanol:methanol (1:1; v/v) solution for LC–MS analysis. Separation was performed by reversed-phase ion-pairing chromatography on a C8 column coupled to negative-ion mode, full-scan LC–MS at 1-Hz scan time and 100,000 resolving power (stand-alone orbitrap; Thermo Fischer Scientific). Data analysis with MAVEN software and natural isotope correction were performed as previously described⁴⁰.

Primary hepatocyte isolation

Hepatocytes were isolated using a two-step collagenase and DNase digestion protocol⁴¹ and plated in M199 media containing 5 mM glucose, 10% FBS, 500 nM dexamethasone and 1 nM insulin. After attachment, cells were changed to M199 media containing 5 mM glucose, 500 nM dexamethasone and incubated overnight. Cells were switched to M199 containing 5 mM glucose, 10% FBS, 500 nM dexamethasone, 100 nM insulin and respective fructose and acetate supplementation for 6 h on the day of experiment. Evidence that high concentrations of glucose are required to induce the DNL gene program in primary hepatocytes⁴² informed our use of 25 mM fructose.

Acyl-CoA measurements in primary hepatocytes

Measurements of Acyl-CoA in primary hepatocytes were performed by LC–MS/high-resolution mass spectrometry as previously described⁴³. In brief, primary hepatocytes were isolated and cultured in 6-well plates as described in ‘Primary hepatocyte isolation’. At collection, culture medium was completely aspirated before collecting cells in 0.5 ml ice-cold 10% trichloroacetic acid per well of a 6-well dish using a cell lifter. Samples were then sonicated for 10 \times 0.5 s pulses to completely disrupt cellular membranes, and incubated on ice to precipitate proteins. Protein was pelleted at 16,000g for 10 min at 4 °C. Supernatant was collected and purified by solid-phase extraction using Oasis HLB 1cc (30 mg) SPE columns (Waters). Eluate was evaporated to dryness under nitrogen gas and re-suspended in 50 μ l of 5% 5-sulfosalicylic acid (w/v) for injection. Samples were analysed by an Ultimate 3000 autosampler coupled to a Thermo Q-Exactive Plus instrument in positive electrospray ionization (ESI) mode. For isotopic tracer analysis, isotopic enrichment from [U - ^{13}C]fructose (Cambridge Isotope Laboratories, CLM-1553) or [U - ^{13}C]acetate (Cambridge Isotope Laboratories, CLM-440-1) was calculated to compensate for the nonlinearity of isotopic enrichment using the FluxFix calculator⁴⁴.

Fructolytic measurements in primary hepatocytes

For fructolytic intermediate measurements in primary hepatocytes, culture medium was completely aspirated before collecting cells in 0.5 ml of cold 80:20 methanol:water per well of a 6-well dish using a cell lifter. Samples were then sonicated for 10 \times 0.5-s pulses to completely disrupt cellular membranes, and incubated on ice. Samples were then spun down at 16,000g for 10 min at 4 °C. Supernatant was collected and dried under nitrogen gas flow in preparation for water-soluble metabolomic analysis.

ChIP–qPCR

For H3K27ac ChIP–qPCR studies, wild-type male mice were provided with fructose:glucose drinking water for 24 h, and orally gavaged with 2.0 g kg⁻¹ fructose plus 2.0 g kg⁻¹ glucose 1 h before being euthanized. ChIP was performed as previously described⁴⁵ with adjustments to start from liver tissue. Liver tissues were obtained from mice 90 min after gavage, and 100 mg of tissue was weighed. Tissues were homogenized by mincing briefly with razor blades followed by resuspension in 5 ml of ice-cold PBS and several passages through a 16-gauge syringe needle into 15-ml conical tubes. Samples were crosslinked with 2% formaldehyde for 10 min at room temperature. The reactions were quenched with 0.25 M glycine. The cells were then washed with PBS and resuspended in cell lysis buffer (10 mM Tris-HCl, pH 8.1, 10 mM NaCl, 1.5 mM MgCl₂, 0.5% NP-40), supplemented with protease inhibitors (Roche). The cell pellet was resuspended in 0.5 ml of nuclear lysis buffer (50 mM Tris-HCl pH 8.1, 5 mM EDTA, 1% SDS) supplemented with protease inhibitors. The chromatin was fragmented with a Diagenode Bioruptor Pico (12 cycles of 30 s on followed by 30 s off, at 4 °C). Samples were incubated with protein G magnetic beads (Millipore-Sigma, 16-662) and H3K27ac (Abcam, ab4729) or normal rabbit IgG (Cell Signalling Technology, 2729S) antibody overnight at 4 °C. The next day, samples were washed five times with decreasingly stringent buffers. ChIP DNA was eluted off the beads by incubating beads in 125 μ l elution buffer for 10 min at 65 °C. The combined supernatant was then incubated overnight at 65 °C to reverse crosslinks and treated with proteinase K for 1 h the next morning. Samples were purified using Macherey-Nagel DNA purification kit, with NTB binding buffer. Samples were diluted 1:5 in nuclease-free water before RT–qPCR reactions, which were performed as described above with the following primers: *Mlxip1* p1 (forward: CGCACCCGGTCTACAGTTT, reverse: GTGCCTCTCTCTCCTT AGC), *Mlxip1* p2 (forward: GCCATCCACGTGCTAAGGA, reverse: GGCTTTTACTGGGGTGTGG), *Pklr* p1 (forward: GGGAGGATGCCCA CTACAG, reverse: TTGGAAGCCTTGACTACTGGG), *Pklr* p2 (forward: CCCAGTGACAAGGCTCCAT, reverse: CTCTGCCTTTGTCAGTGGGA), *Acss2* p1 (forward: ATTGGATGCCTAGACACGG, reverse: CGCATCAAGT TCCGAACACC), *Acss2* p2 (forward: TCAGGACAGTTTAGGGTGCAA, Reverse: TTACAAAGACCTGCCTCTGCC).

Triglyceride measurements

Triglyceride measurements were performed using a Triglyceride Colorimetric Assay Kit (Cayman Chemical, 10010303) as per manufacturer’s instructions.

Metabolomics

Water-soluble metabolite extraction was performed as previously described⁹. For serum samples, 100 μ l of methanol at –20 °C was added to 5 μ l of serum sample and incubated on ice for 10 min, followed by vortexing and centrifugation at 16,000g for 10 min at 4 °C. The supernatant (first extract) was transferred to a new tube. Then, 50 μ l methanol was added to resuspend the pellet, followed by vortexing and centrifugation at 16,000g for 10 min at 4 °C. The supernatant (second extract) was combined with the first extract. Then, 3 μ l of the 150 μ l extract was loaded to LC–MS. For tissue samples, frozen tissue samples were ground at liquid nitrogen temperature with a Cryomill (Retsch). The resulting tissue powder was weighed (approximately 20 mg). The extraction was then done by adding –20 °C 40:40:20 methanol:acetonitrile:water to the powder and incubating at –20 °C overnight, followed by vortexing and centrifugation at 16,000g for 10 min at 4 °C. The volume of the extraction solution (μ l) was 40 \times the weight of tissue (mg) to make an extract of 25 mg tissue per millilitre solvent. Serum and tissue extracts were analysed by LC–MS, using two different LC–MS methods chosen for optimal separation of glucose and fructose (in serum) and of hexose phosphate species (from tissues). Serum extracts were analysed (without drying) using a quadrupole-orbitrap mass spectrometer (Q Exactive, Thermo Fisher Scientific)

Article

operating in negative ion mode, coupled to hydrophilic interaction chromatography via electrospray ionization and used to scan from m/z 70 to 1000 at 1 Hz and 75,000 resolution. Liquid chromatography separation was on a XBridge BEH Amide column (2.1 mm \times 150 mm, 2.5 μ m particle size, 130 Å pore size) using a gradient of solvent A (20 mM ammonium acetate, 20 mM ammonium hydroxide in 95:5 water: acetonitrile, pH 9.45) and solvent B (acetonitrile). Flow rate was 150 μ l min⁻¹. The liquid chromatography gradient was: 0 min, 85% B; 2 min, 85% B; 3 min, 80% B; 5 min, 80% B; 6 min, 75% B; 7 min, 75% B; 8 min, 70% B; 9 min, 70% B; 10 min, 50% B; 12 min, 50% B; 13 min, 25% B; 16 min, 25% B; 18 min, 0% B; 23 min, 0% B; 24 min, 85% B; 30 min, 85% B. Autosampler temperature was 5 °C, and injection volume was 3 μ l. Tissue extracts were dried under nitrogen gas flow and re-dissolved in LC-MS grade water. Metabolites were analysed via reverse-phase ion-pairing chromatography coupled to an Exactive Orbitrap mass spectrometer (Thermo Fisher Scientific). The mass spectrometer was operated in negative ion mode with resolving power of 100,000 at m/z 200 and scan range of m/z 75–1000. The liquid chromatography method was modified from an earlier method⁴⁶, using an Atlantis T3 column (150 mm \times 2.1 mm, 3 μ m particle size, 100 Å pore size), with a gradient of solvent A (97:3 water:methanol with 10 mM tributylamine and 15 mM acetic acid) and solvent B (methanol). The liquid chromatography gradient was 0 min, 0% B, 200 μ l min⁻¹; 2 min, 0% B, 200 μ l min⁻¹; 4 min, 20% B, 200 μ l min⁻¹; 13 min, 80% B, 200 μ l min⁻¹; 17 min, 100% B, 200 μ l min⁻¹; 17.5 min, 100% B, 300 μ l min⁻¹; 20 min, 100% B, 300 μ l min⁻¹; 20.5 min, 0% B, 300 μ l min⁻¹; 24 min, 0% B, 300 μ l min⁻¹; 25 min, 0% B, 200 μ l min⁻¹. Other liquid chromatography parameters, common to both methods, were column temperature 25 °C, autosampler temperature 5 °C, and injection volume 10 μ l. Data analysis with MAVEN software and natural isotope correction was performed as previously described⁴⁰. Volcano plot and principle component analysis of metabolomics data were generated using Metaboanalyst⁴⁷.

Acetate measurement

Acetate was derivatized and measured by LC-MS. The derivatization mixture was 12 mM EDC, 15 mM 3-nitrophenylhydrazine and pyridine (2% v/v) in methanol. The reaction was stopped with quenching reagent consisting of 0.5 mM β -mercaptoethanol in water. Serum (5 μ l) was mixed with derivatizing reagent (100 μ l) and incubated for 1 h at 4 °C. Then, the samples were centrifuged at 16,000g for 10 min at 4 °C, and 20 μ l of supernatant was mixed with 200 μ l of the quenching reagent. After centrifugation at 16,000g for 10 min at 4 °C, supernatants were collected for LC-MS analysis. A quadrupole-time-of-flight mass spectrometer (Agilent 6550 iFunnel Q-TOF) operating in negative ion mode was coupled to C18 chromatography via electrospray ionization and used to scan from m/z 100 to 300 at 1 Hz and 15,000 resolution. Liquid chromatography separation was on an Acquity UPLC BEH C18 column (2.1 mm \times 100 mm, 1.75 μ m particle size, 130 Å pore size; Waters) using a gradient of solvent A (water) and solvent B (methanol). Flow rate was 200 μ l min⁻¹. The liquid chromatography gradient was: 0 min, 10% B; 1 min, 10% B; 5 min, 30% B; 7 min, 100% B; 11 min, 100% B; 11.5 min, 10% B; 14 min, 10% B. Autosampler temperature was 5 °C, column temperature was 60 °C, and injection volume was 10 μ l. Ion masses for derivatized acetate were 194.

Lipidomics

Lipidomics was performed as previously described⁴⁸, with some modifications on an extraction step. In brief, liver powder (10 mg) was dissolved in 100 μ l of isopropanol. After centrifugation at 14,000g at 4 °C for 10 min, supernatant was transferred to a glass mass spectrometry vial and injected into a 1290 Infinity UHPLC system coupled to the Q-TOF mass spectrometer (the same instrument as used for acetate measurement). To cover both the positive charged and negative charged species, each sample was analysed twice using the same liquid chromatography gradient but with different mass spectrometer ionization modes. The liquid chromatography separation was performed on an Agilent Poroshell 120 EC-C18 column (150 \times 2.1 mm, 2.7 μ m particle

size) with a flow rate of 150 μ l min⁻¹. Solvent A was 1 mM ammonium acetate plus 0.2% acetic acid in water/methanol (90:10). Solvent B was 1 mM ammonium acetate plus 0.2% acetic acid in methanol/2-propanol (2:98). The solvent gradient in volume ratios was as follows: 0–2 min, 25% B; 2–4 min, 25 to 65% B; 4–16 min, 65 to 100% B; 16–20 min, 100% B; 20–21 min, 100 to 25% B; 21–27 min, 25% B. Principle component analysis was generated using Metaboanalyst⁴⁷ (<https://www.metaboanalyst.ca>) and a heat map of lipidomics data was generated using Morpheus (<https://software.broadinstitute.org/morpheus>).

Reporting summary

Further information on research design is available in the Nature Research Reporting Summary linked to this paper.

Data availability

All data generated or analysed during this study are included in this published article (and its Supplementary Information files). Source Data for Figs. 1–4 and Extended Data Figs. 1, 4–9 are provided with the paper.

- Postic, C. et al. Dual roles for glucokinase in glucose homeostasis as determined by liver and pancreatic beta cell-specific gene knock-outs using Cre recombinase. *J. Biol. Chem.* **274**, 305–315 (1999).
- Nadkarni, M. A., Martin, F. E., Jacques, N. A. & Hunter, N. Determination of bacterial load by real-time PCR using a broad-range (universal) probe and primers set. *Microbiology* **148**, 257–266 (2002).
- Guan, D. et al. Diet-induced circadian enhancer remodeling synchronizes opposing hepatic lipid metabolic processes. *Cell* **174**, 831–842.e12 (2018).
- Su, X., Lu, W. & Rabinowitz, J. D. Metabolite Spectral Accuracy on Orbitraps. *Anal. Chem.* **89**, 5940–5948 (2017).
- Titchenell, P. M., Chu, Q., Monks, B. R. & Birnbaum, M. J. Hepatic insulin signalling is dispensable for suppression of glucose output by insulin in vivo. *Nat. Commun.* **6**, 7078 (2015).
- Iroz, A. et al. A specific ChREBP and PPAR α cross-talk is required for the glucose-mediated FGF21 response. *Cell Rep.* **21**, 403–416 (2017).
- Frey, A. J. et al. LC-quadrupole/Orbitrap high-resolution mass spectrometry enables stable isotope-resolved simultaneous quantification and ¹³C-isotopic labeling of acyl-coenzyme A thioesters. *Anal. Bioanal. Chem.* **408**, 3651–3658 (2016).
- Trefely, S., Ashwell, P. & Snyder, N. W. FluxFix: automatic isotopologue normalization for metabolic tracer analysis. *BMC Bioinformatics* **17**, 485 (2016).
- Lee, J. V. et al. Acetyl-CoA promotes glioblastoma cell adhesion and migration through Ca²⁺-NFAT signaling. *Genes Dev.* **32**, 497–511 (2018).
- Lu, W. et al. Metabolomic analysis via reversed-phase ion-pairing liquid chromatography coupled to a stand alone orbitrap mass spectrometer. *Anal. Chem.* **82**, 3212–3221 (2018).
- Chong, J. et al. MetaboAnalyst 4.0: towards more transparent and integrative metabolomics analysis. *Nucleic Acids Res.* **46** (W1), W486–W494 (2018).
- Neinast, M. D. et al. Quantitative analysis of the whole-body metabolic fate of branched-chain amino acids. *Cell Metab.* **29**, 417–429.e4 (2018).

Acknowledgements This work was supported by grants R01CA174761, R01CA228339 and R01DK116005 to K.E.W. S.Z. is supported by pre-doctoral fellowship F99CA222741. C.J. is supported by the American Diabetes Association through post-doctoral fellowship 1-17-PDF-076. K.U. is supported by NIAMS training grant T32AR053461. L.I. is supported by NIGMS training grant T32GM07229. S.T. is supported by the American Diabetes Association through post-doctoral fellowship 1-18-PDF-144. S.F. is supported through the Penn-PORT IRACDA grant K12 GM081259. P.M.T. is supported by K01DK111715. N.W.S. is supported by the NIH grant R03HD092630 and R01GM132261. J.D.R. is supported by the NIH Pioneer Award 1DP1DK113643 and Diabetes Research Center P30 DK019525. We thank S. Berger and P. Mews for providing the AAV.U6.shAcsc2.CMV.eGFP.SV40 vector. We thank G. Wu and Y. Saimon for discussions on the microbiome.

Author contributions The project was conceptualized and designed by S.Z., C.J. and K.E.W. K.E.W. and J.D.R. guided the study. S.Z. generated LAKO mice and performed most of the mouse experiments, with help from J.L., S.F., A.C. and K.D.M. C.J. performed mouse experiments and most of the LC-MS analyses with help from X.Z. for LC-MS analysis of short-chain fatty acid species. S.T. and N.W.S. performed LC-MS analysis of acyl-CoA species. K.U. isolated and performed experiments on primary hepatocytes. J.L., M.G. and L.I. performed experiments. P.M.T., Z.T.S. and T.P.G. provided guidance on study design. S.Z. prepared figures with input from C.J., J.D.R. and K.E.W. S.Z., C.J. and K.E.W. wrote and edited the manuscript, with input from J.D.R. All authors read and provided feedback on manuscript and figures.

Competing interests J.D.R. is a consultant to Pfizer and to Colorado Research Partners. All other authors declare no conflicts of interest.

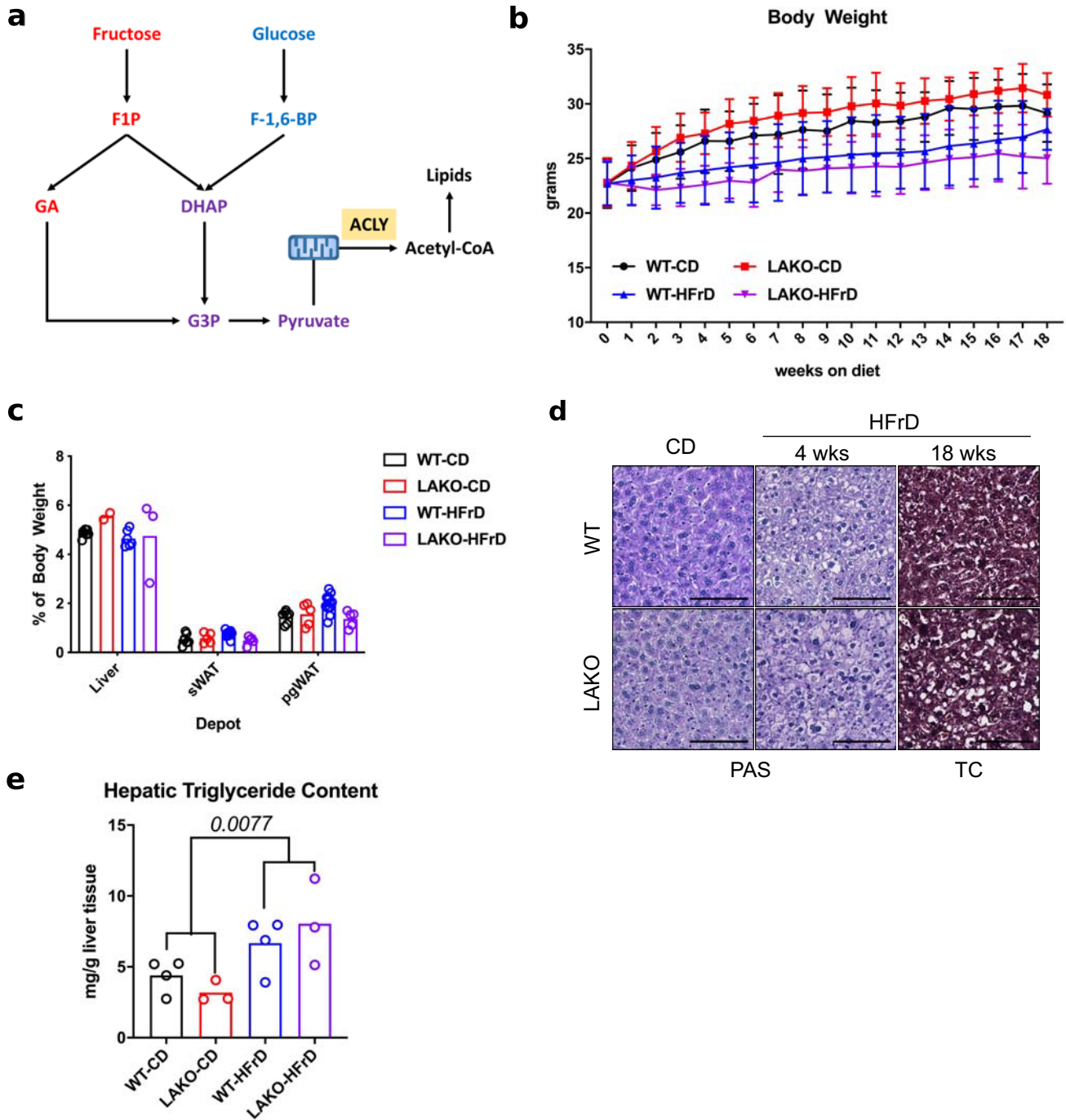
Additional information

Supplementary information is available for this paper at <https://doi.org/10.1038/s41586-020-2101-7>.

Correspondence and requests for materials should be addressed to K.E.W.

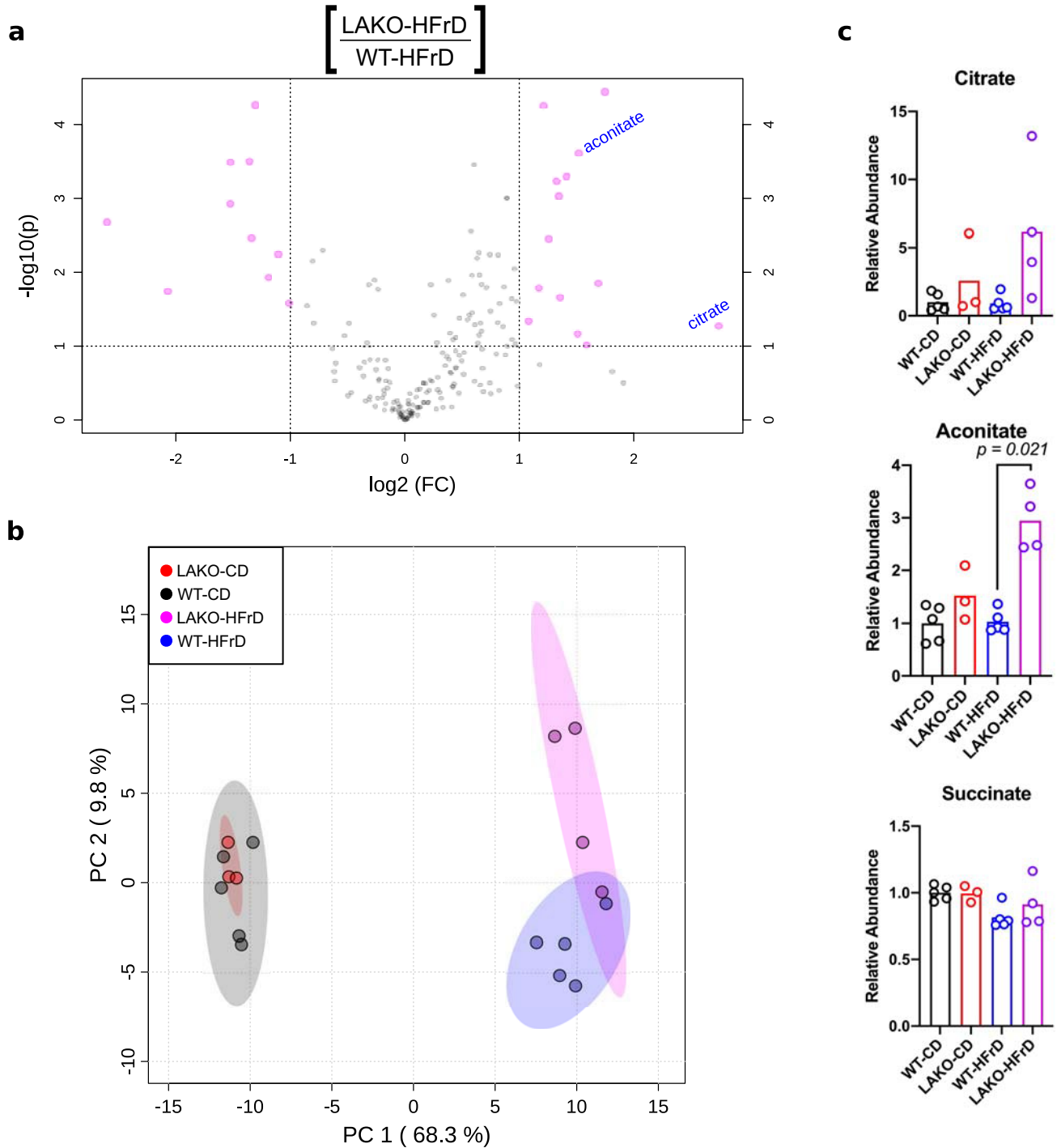
Peer review information Nature thanks D. Wade Abbott, Navdeep Chandel, Catherine Postic and the other, anonymous, reviewer(s) for their contribution to the peer review of this work.

Reprints and permissions information is available at <http://www.nature.com/reprints>.



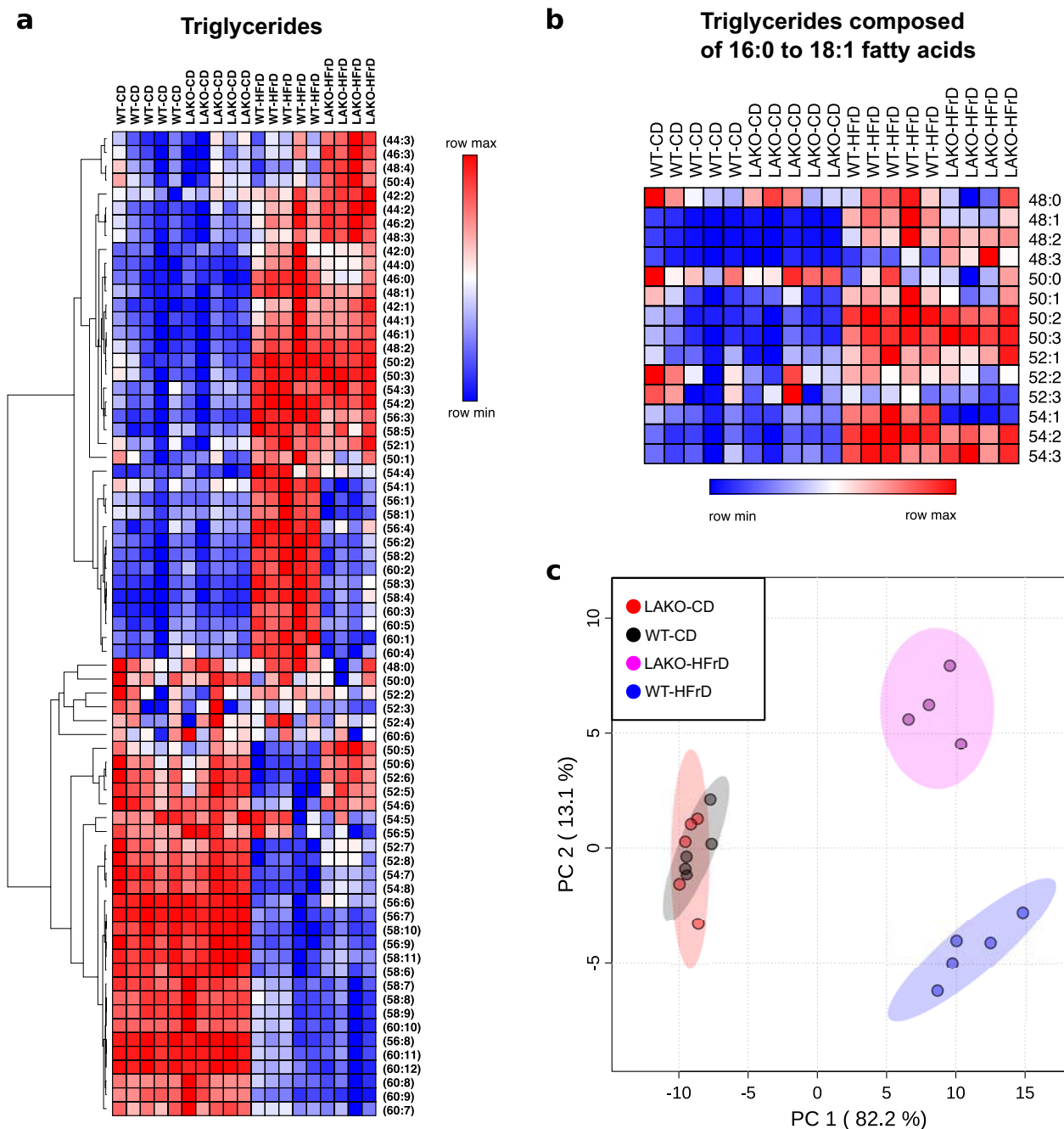
Extended Data Fig. 1 | Hepatic ACLY deficiency minimally affects the response to dietary fructose. **a**, Schematic of fructolysis and glycolysis feeding into de novo lipogenesis. **b**, Body weights of wild-type and LAKO mice fed a chow diet (CD) or high-fructose diet (HFrD) for 18 weeks ($n = 13$ WT-CD; $n = 5$ LAKO-CD; $n = 14$ WT-HFrD; and $n = 5$ LAKO-HFrD mice). Data are mean \pm s.d. **c**, Weights of liver, posterior subcutaneous white adipose tissue (sWAT) and perigonadal adipose tissue (pgWAT) in wild-type and LAKO mice on a chow diet or HFrD for 18 weeks (liver/sWAT/pgWAT: $n = 7/7/7$ WT-CD; $n = 2/5/5$ LAKO-CD;

$n = 6/12/12$ WT-HFrD; and $n = 3/5/5$ LAKO-HFrD). **d**, Representative histology images of Periodic acid–Schiff (PAS) stain for glycogen and trichrome (TC) for fibrosis in livers from wild-type or LAKO mice on a HFrD. Scale bars, 100 μ m. Images are representative of two mice per group in one experiment. **e**, Triglyceride content in wild-type or LAKO mice on a chow diet or HFrD for 18 weeks ($n = 4$ WT-CD; $n = 3$ LAKO-CD; $n = 3$ WT-HFrD; $n = 4$ LAKO-HFrD). P values determined by Welch's t -test. Data in **c** and **e** denote mean values.



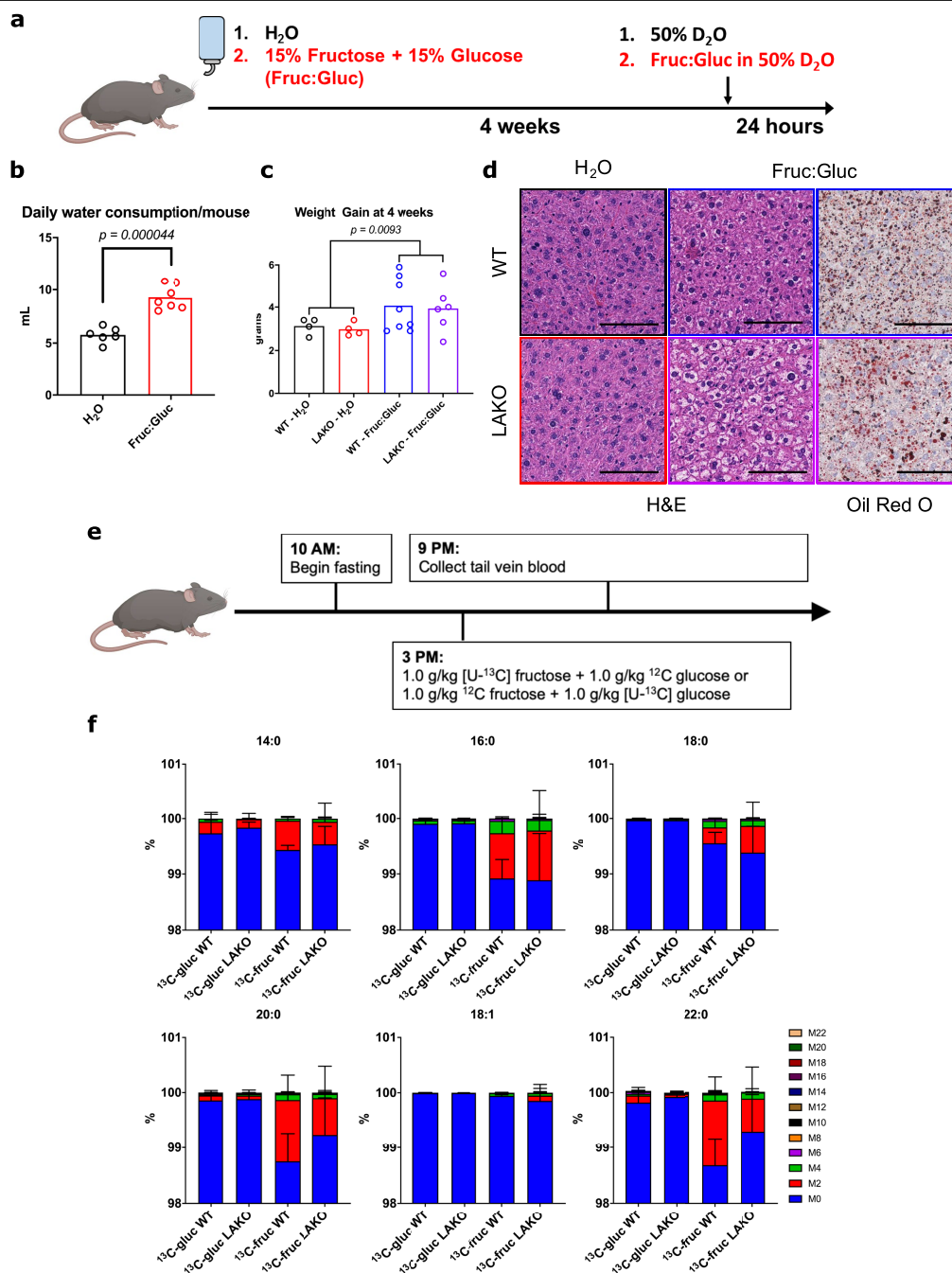
Extended Data Fig. 2 | Hepatic ACLY deficiency results in modest metabolic alterations on a high-fructose diet. **a**, Volcano plot of hepatic metabolites in wild-type or LAKO mice on a chow (CD) or high-fructose diet (HFrD) for 4 weeks. Pink dots indicate significant hits as determined by a fold-change (FC) threshold of 2.0, and *P*-value threshold of 0.1, assuming equal variance. **b**, Principle component (PC) analysis of log-transformed data in

Supplementary Table 1. Each dot represents a unique sample; coloured shading denotes 95% confidence intervals. **c**, Relative abundance of metabolites, normalized to the wild-type chow-diet-fed (WT-CD) group. *P* values determined by Welch's *t*-test (*n* = 5 WT-CD; *n* = 3 LAKO-CD; *n* = 5 WT-HFrD; and *n* = 4 LAKO-HFrD mice). Data are mean values.



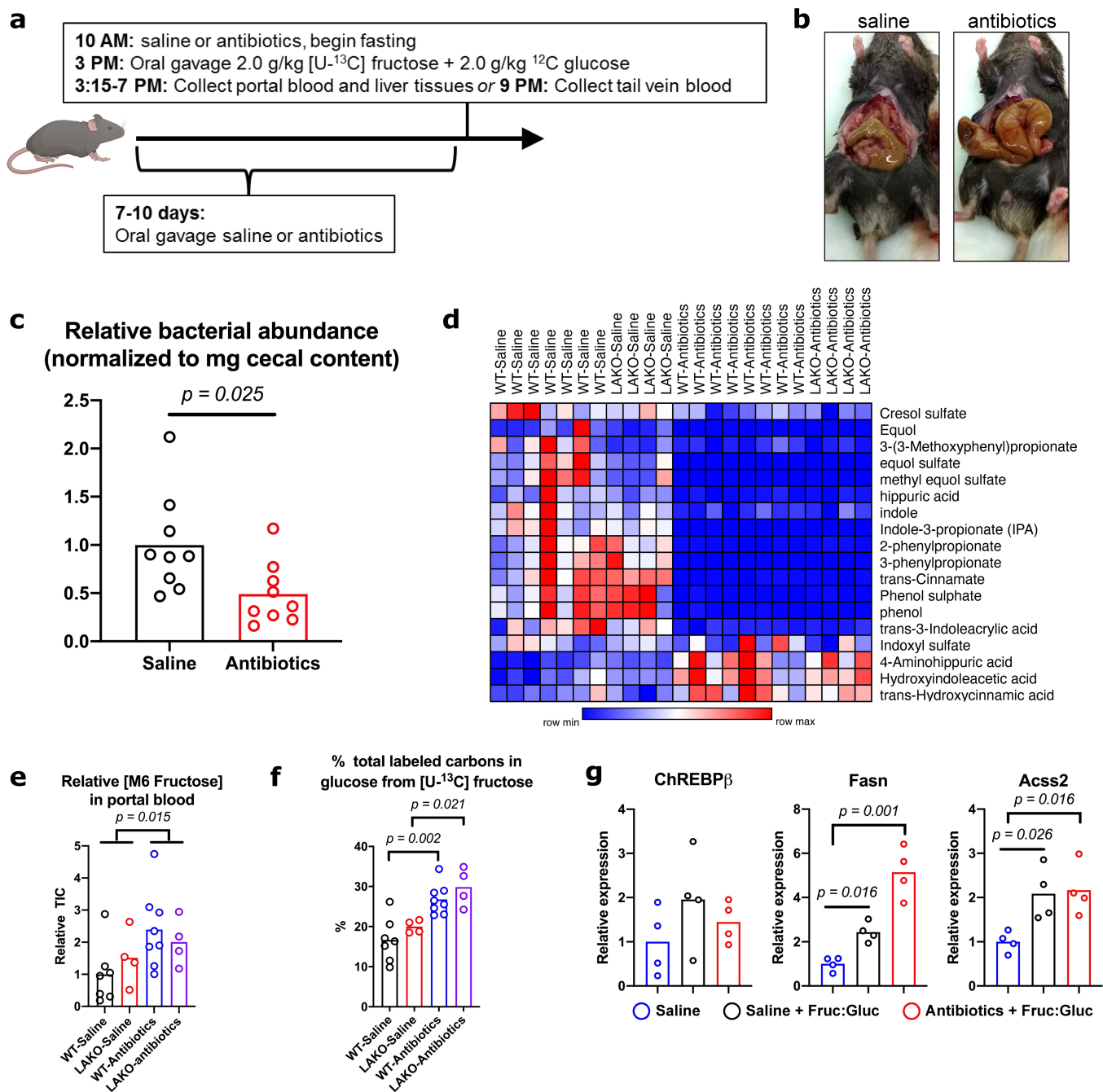
Extended Data Fig. 3 | A high-fructose diet alters hepatic lipid metabolism.
a, Hierarchical clustering of relative hepatic triglyceride abundance in wild-type or LAKO mice on a chow diet (CD) or high fructose diet (HFrD) for 4 weeks. Clustering performed using 1–Pearson’s correlation and average linkage.

b, Relative abundance of hepatic triglycerides composed of 16:0 to 18:1 fatty acids; a subset of the data in **a**. **c**, Principle component analysis of log-transformed data in Supplementary Table 2. Each dot represents a unique sample; coloured shading denotes 95% confidence intervals.



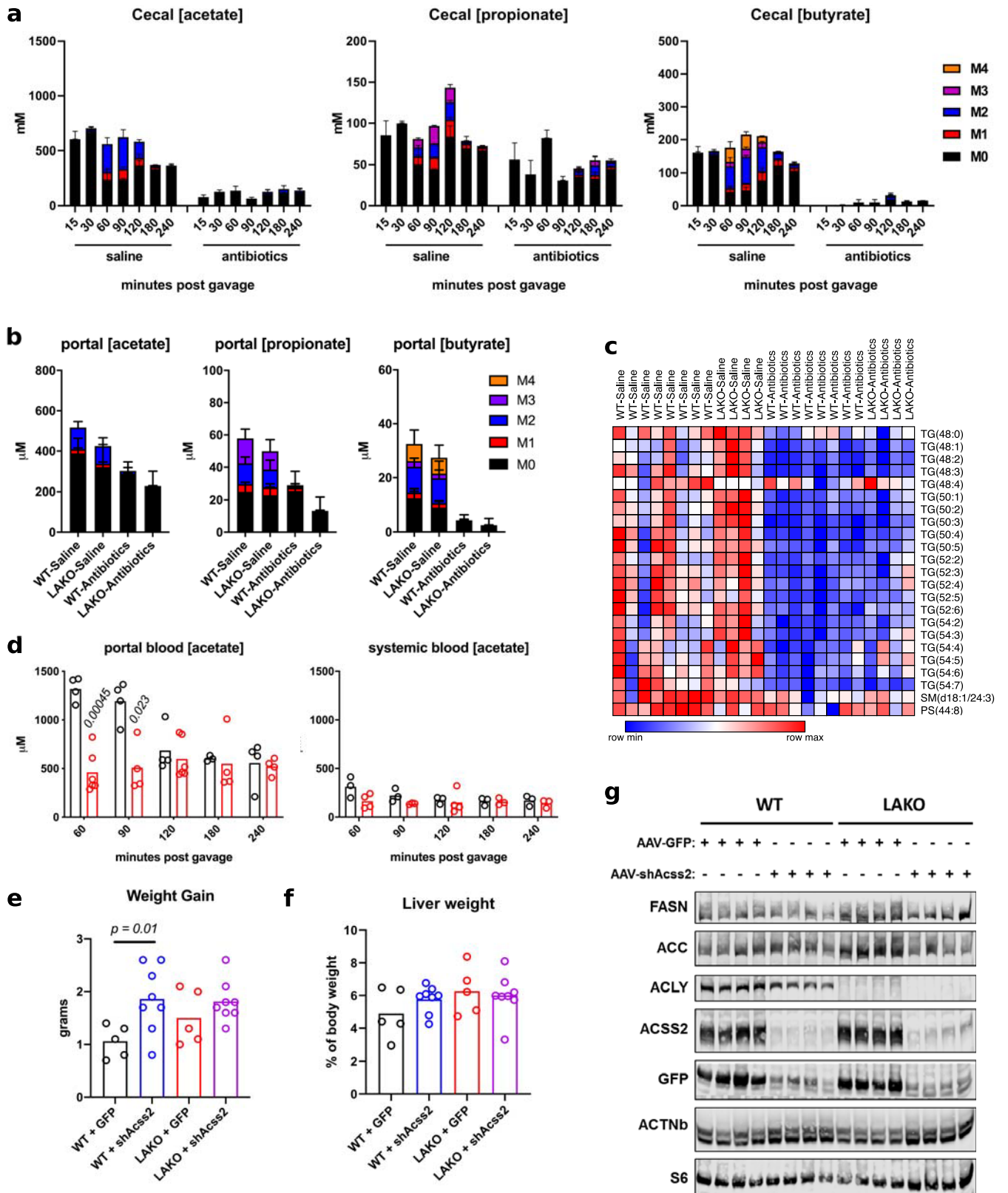
Extended Data Fig. 4 | Fructose induces steatosis and contributes substantially to newly synthesized fatty acids in the liver independently of ACLY. **a**, Schematic of experimental design of the drinking water study. **b**, Daily consumption of unsweetened (H₂O) or 15% fructose and 15% glucose sweetened (Fruc:Gluc) water per mouse. Each dot represents a repeat measurement, and mean values are shown ($n = 6$ H₂O, $n = 7$ Fruc:Gluc). P values determined by Welch's t -test. **c**, Weight gain of wild-type or LAKO mice given water or

fructose:glucose for 4 weeks ($n = 4$ WT-H₂O, LAKO-H₂O; $n = 8$ WT-Fruc:Gluc; and $n = 6$ LAKO-Fruc:Gluc mice). P values comparing all H₂O versus fructose:glucose mice determined by Welch's t -test. **d**, Representative H&E and Oil Red O histological stains of livers from mice in **c**. Scale bars, 100 μ m. **e**, Experimental design for data in Fig. 1c. [U-¹³C] denotes uniformly labelled ¹³C. **f**, Isotopologue distribution of labelled saponified fatty acids in serum shown in Fig. 1c. Data are mean \pm s.d.



Extended Data Fig. 6 | Depletion of microbiota blocks substrate contribution, but not signalling component, of de novo lipogenesis after fructose consumption. **a**, Experimental set-up for antibiotic depletion of the microbiome followed by [¹³C]fructose tracing into DNL. [U-¹³C] denotes uniformly labelled ¹³C. **b**, Representative images of caecums from a mouse treated with saline or antibiotics. **c**, Relative abundance of bacteria in caecal contents from mice treated with saline ($n = 9$) or antibiotics ($n = 9$), as determined by 16S RT-qPCR to a reference standard of *Escherichia coli* DNA. P value determined using Welch's t -test. **d**, Heat map of microbial metabolite

abundance in the portal blood, collected 1 h after gavage. **e, f**, Relative abundance of [¹³C]fructose (**e**) and percentage of total labelled carbons in glucose (**f**) in portal blood from wild-type or LAKO mice treated with saline or antibiotics, collected 1 h after gavage ($n = 7$ WT-saline, WT-antibiotics; and $n = 4$ LAKO-saline, LAKO-antibiotics). P values determined by Welch's t -test. **g**, mRNA expression of *ChREBPβ*, *Acss2* and *Fasn* in liver collected 1 h after gavage ($n = 4$ mice per group). P values determined by two-sided t -tests with Holm-Sidak method for multiple comparisons. Data in **c** and **e-g** denote mean values.

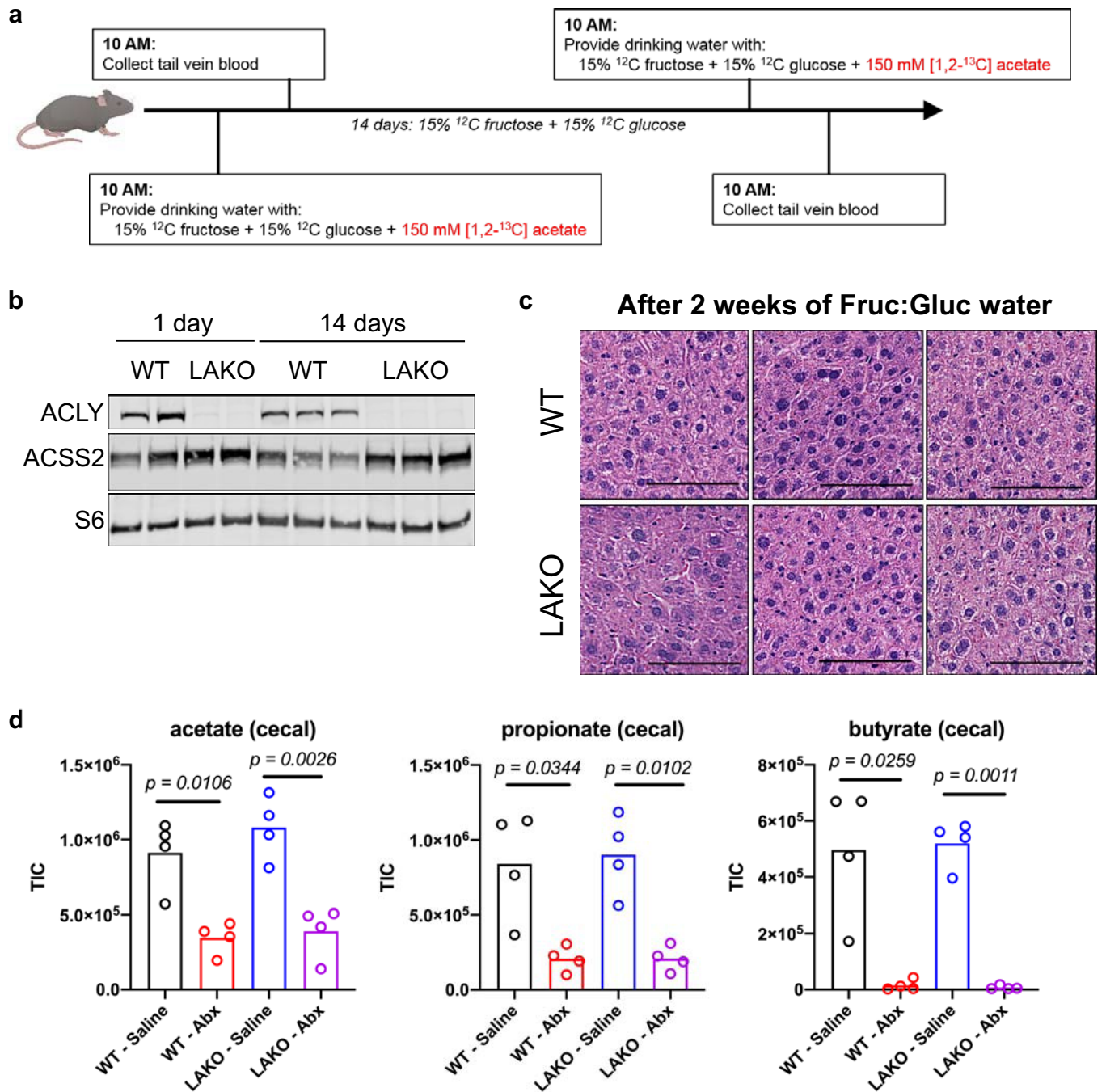


Extended Data Fig. 8 | See next page for caption.

Extended Data Fig. 8 | Bolus fructose-dependent DNL requires microbial acetate and hepatic ACS2. a–d, Mice were gavaged with 2.0 g kg^{-1} [^{13}C]fructose and 2.0 g kg^{-1} unlabelled glucose. **a**, Concentrations of labelled acetate, propionate and butyrate in caecal contents from wild-type mice treated with saline or antibiotics ($n = 3$ mice per time point, except for saline-180 $n = 2$ mice). **b**, Concentrations of labelled acetate, propionate and butyrate in portal blood from wild-type mice treated with saline or antibiotics ($n = 8$ WT-saline, WT-antibiotics; and $n = 4$ LAKO-saline, LAKO-antibiotics), collected 1 h after gavage. **c**, Heat map of hepatic triglyceride abundance in livers of mice treated with saline or antibiotics. **d**, Concentrations of acetate in

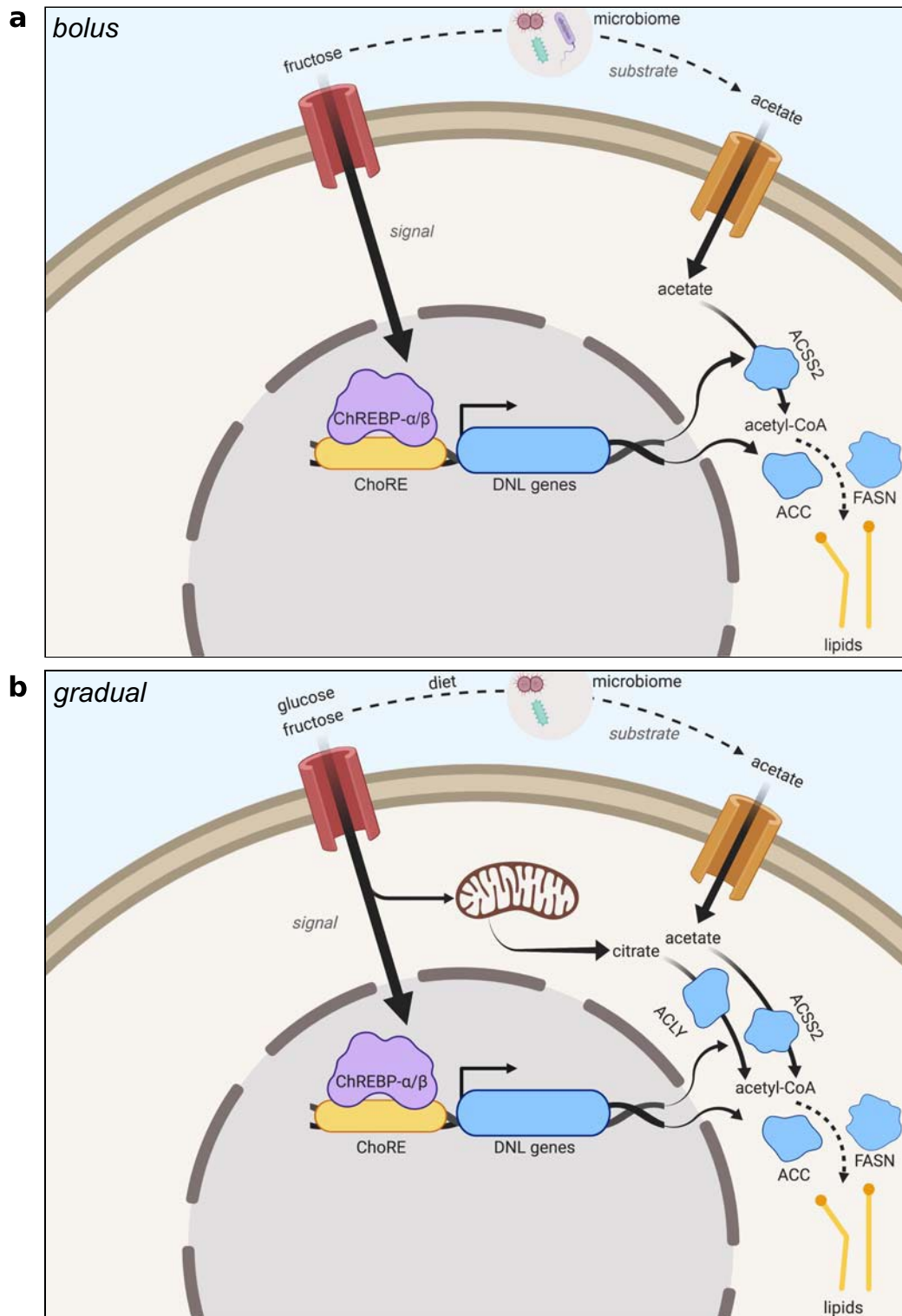
portal and systemic blood after gavage. Each data point represents an individual mouse. *P* value determined by two-sided *t*-tests with Holm–Sidak method for multiple comparisons. **e**, Weight gain in wild-type and LAKO mice 1 week after tail-vein injection of AAV8-GFP or AAV8-shAcsc2. *P* value determined by Welch's *t*-test. **f**, Liver weight of wild-type and LAKO mice as a percentage of body weight 1 week after tail-vein injection of AAV8-GFP or AAV8-shAcsc2. **g**, Western blots of lipogenic enzymes in liver lysates from wild-type and LAKO mice 1 week after tail-vein injection of AAV8-GFP or AAV8-shAcsc2. S6 was used as a loading control.

Article



Extended Data Fig. 9 | Gradual fructose consumption promotes greater acetate usage in LAKO mice. **a**, Experimental set-up for tracing of [1,2-¹³C]acetate into DNL before and after gradual administration of fructose. [1,2-¹³C] denotes ¹³C labelling of 1 and 2 position carbons in acetate. **b**, Western blots of lipogenic enzymes in liver lysates from wild-type and LAKO mice after being given fructose:glucose water for 1 or 14 days. **c**, Representative H&E

stains of livers from wild-type and LAKO mice provided fructose:glucose water for 2 weeks. Scale bars, 100 μ m. **d**, Relative abundance of acetate, propionate and butyrate in the caecal contents of wild-type and LAKO mice treated with saline or antibiotics for 1 week ($n = 4$ mice per group). P values determined by Welch's t -test.



Extended Data Fig. 10 | Fructose provides signal and substrate to promote hepatic DNL. a. Proposed model of bolus fructose-induced hepatic DNL. Fructose catabolism in hepatocytes acts as a signal to induce DNL genes including *Acsc2*, whereas fructose metabolism by the gut microbiota provides acetate as a substrate to feed DNL, which is mediated by *ACS2*. **b.** Proposed model of gradual fructose-induced hepatic DNL. Similar to the bolus model,

fructose catabolism in hepatocytes acts as a signal to induce DNL genes. Catabolism of hepatic fructose and glucose (made from fructose by the small intestine) provides citrate as a substrate to feed DNL, which is mediated by *ACLY*. Metabolism of fibres and other dietary components by the gut microbiota provides acetate as a substrate to feed DNL, after its conversion to acetyl-CoA by hepatic *ACS2*. Image created with BioRender.com.

Reporting Summary

Nature Research wishes to improve the reproducibility of the work that we publish. This form provides structure for consistency and transparency in reporting. For further information on Nature Research policies, see [Authors & Referees](#) and the [Editorial Policy Checklist](#).

Statistics

For all statistical analyses, confirm that the following items are present in the figure legend, table legend, main text, or Methods section.

n/a Confirmed

- The exact sample size (n) for each experimental group/condition, given as a discrete number and unit of measurement
- A statement on whether measurements were taken from distinct samples or whether the same sample was measured repeatedly
- The statistical test(s) used AND whether they are one- or two-sided
Only common tests should be described solely by name; describe more complex techniques in the Methods section.
- A description of all covariates tested
- A description of any assumptions or corrections, such as tests of normality and adjustment for multiple comparisons
- A full description of the statistical parameters including central tendency (e.g. means) or other basic estimates (e.g. regression coefficient) AND variation (e.g. standard deviation) or associated estimates of uncertainty (e.g. confidence intervals)
- For null hypothesis testing, the test statistic (e.g. F , t , r) with confidence intervals, effect sizes, degrees of freedom and P value noted
Give P values as exact values whenever suitable.
- For Bayesian analysis, information on the choice of priors and Markov chain Monte Carlo settings
- For hierarchical and complex designs, identification of the appropriate level for tests and full reporting of outcomes
- Estimates of effect sizes (e.g. Cohen's d , Pearson's r), indicating how they were calculated

Our web collection on [statistics for biologists](#) contains articles on many of the points above.

Software and code

Policy information about [availability of computer code](#)

Data collection

Data collection for metabolomics was done using Xcaliber Qual Browser (Thermo Fisher) and TraceFinder (Thermo Fisher)

Data analysis

Data analysis was performed using MAVEN, FluxFix, and GraphPad Prism versions 7 and 8.

For manuscripts utilizing custom algorithms or software that are central to the research but not yet described in published literature, software must be made available to editors/reviewers. We strongly encourage code deposition in a community repository (e.g. GitHub). See the Nature Research [guidelines for submitting code & software](#) for further information.

Data

Policy information about [availability of data](#)

All manuscripts must include a [data availability statement](#). This statement should provide the following information, where applicable:

- Accession codes, unique identifiers, or web links for publicly available datasets
- A list of figures that have associated raw data
- A description of any restrictions on data availability

All data generated or analysed during this study are included in this published article (and its supplementary information files).

Field-specific reporting

Please select the one below that is the best fit for your research. If you are not sure, read the appropriate sections before making your selection.

- Life sciences Behavioural & social sciences Ecological, evolutionary & environmental sciences

For a reference copy of the document with all sections, see nature.com/documents/nr-reporting-summary-flat.pdf

Life sciences study design

All studies must disclose on these points even when the disclosure is negative.

Sample size	Sample sizes were determined in accordance with the literature and based on previous experience in our group.
Data exclusions	No data were excluded from the analyses in this study.
Replication	Experimental findings were verified by using multiple mice in each study as replicates. Replications were successful.
Randomization	Mice of different genotypes were randomly assigned to treatment groups throughout this study.
Blinding	Sample preparation and data acquisition for metabolomics were performed in a blinded manner.

Reporting for specific materials, systems and methods

We require information from authors about some types of materials, experimental systems and methods used in many studies. Here, indicate whether each material, system or method listed is relevant to your study. If you are not sure if a list item applies to your research, read the appropriate section before selecting a response.

Materials & experimental systems

n/a	Involved in the study
<input type="checkbox"/>	<input checked="" type="checkbox"/> Antibodies
<input checked="" type="checkbox"/>	<input type="checkbox"/> Eukaryotic cell lines
<input checked="" type="checkbox"/>	<input type="checkbox"/> Palaeontology
<input type="checkbox"/>	<input checked="" type="checkbox"/> Animals and other organisms
<input checked="" type="checkbox"/>	<input type="checkbox"/> Human research participants
<input checked="" type="checkbox"/>	<input type="checkbox"/> Clinical data

Methods

n/a	Involved in the study
<input checked="" type="checkbox"/>	<input type="checkbox"/> ChIP-seq
<input checked="" type="checkbox"/>	<input type="checkbox"/> Flow cytometry
<input checked="" type="checkbox"/>	<input type="checkbox"/> MRI-based neuroimaging

Antibodies

Antibodies used	ACLY (Proteintech, Catalogue #: 15421-1-AP, Lot: 00040639), ACSS2 (Cell Signaling Technology, Catalogue #: 3658, Clone: D19C6, Lot: 2), ACC (Cell Signaling Technology, Catalogue #: 3676, Clone: C83B10, Lot: 9), FASN (Cell Signaling Technology, Catalogue #: 3189, Lot: 2), CHREBP (Novus Biologicals, Catalogue #: NB400-135, Lot: H-1), IgG (Cell Signaling Technology, Catalogue #: 2729, Lot: 8), CAT (Cell Signaling Technology, Catalogue #: 14097, Clone: D5N7V, Lot: 1), S6 (Cell Signaling Technology, Catalogue #: 2217, Lot: 7), Acetyl-H3K27 (Abcam, Catalogue #: ab4729, Lot: GR3216173-1)
Validation	All antibodies were used in accordance to the manufacturer guidelines and confirmed to have previously been documented in the literature through CiteAb (www.citeab.com).

Animals and other organisms

Policy information about [studies involving animals](#); [ARRIVE guidelines](#) recommended for reporting animal research

Laboratory animals	Mice used in this study were on a C57bl/6j background, all males, and between the ages of 8-12 weeks for acute experiments. Long-term diet studies were started when mice were around 6-8 weeks of age.
Wild animals	This study did not involve wild animals.
Field-collected samples	This study did not involve field-collected samples.
Ethics oversight	All animal protocols in this study were approved by the Institutional Animal Care and Use Committees (IACUC) at the University of Pennsylvania and Princeton University.

Note that full information on the approval of the study protocol must also be provided in the manuscript.